Diamond-II

Opportunities and Challenges for Spectroscopy

Gianluigi Botton

Diamond-II | Advancing Science

Outline

- Diamond-II highlights for spectroscopy
- Current spectroscopy examples where the theory has helped/can help
- A diversion to energy loss spectroscopy
- Summary of opportunities and challenges.

Science Drivers from Users' Community

Imaging

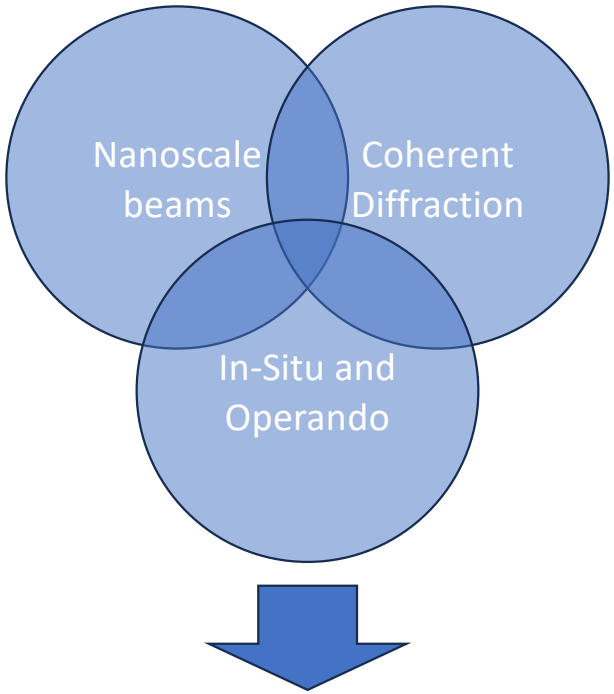

Spectroscopy

Diamond-II upgrade to machine and beamlines

The new lattice to achieve the science

160pm.rad

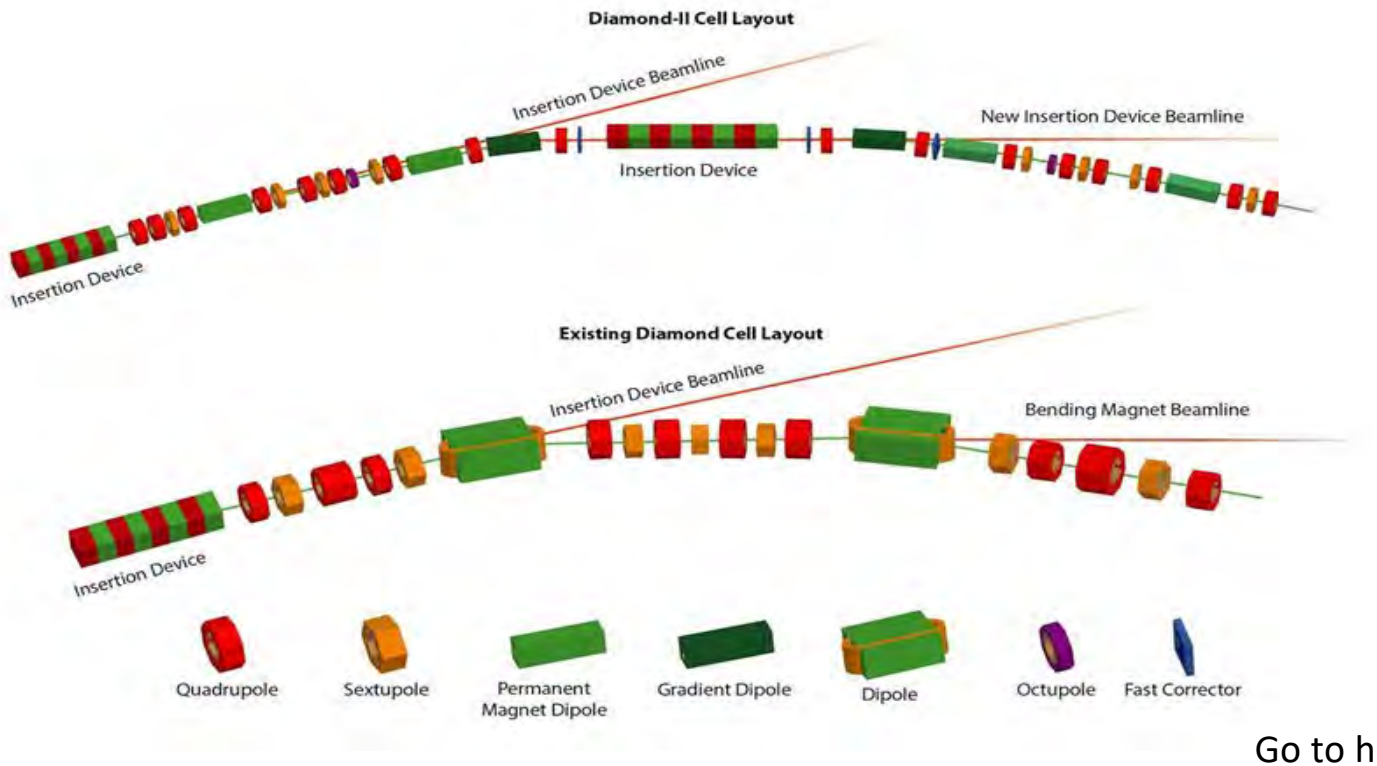

2.7nm.rad

Lower emittance,
Increased capacity,
Higher energies

Go to higher energies 3.5GeV

Figure 1-1 : Schematic of the current Diamond DBA (Double Bend Achromat) lattice (bottom), and the proposed design of a DTBA (Double Triple Bend Achromat) lattice for Diamond-II (top).

Design and changes in energy reduce the emittance by a factor of 20

One dipole replaced by 6 dipoles, smaller fields, lower deflection => lower emittance.

diamond

Diamond-II | Advancing Science

Improvements

Brightness

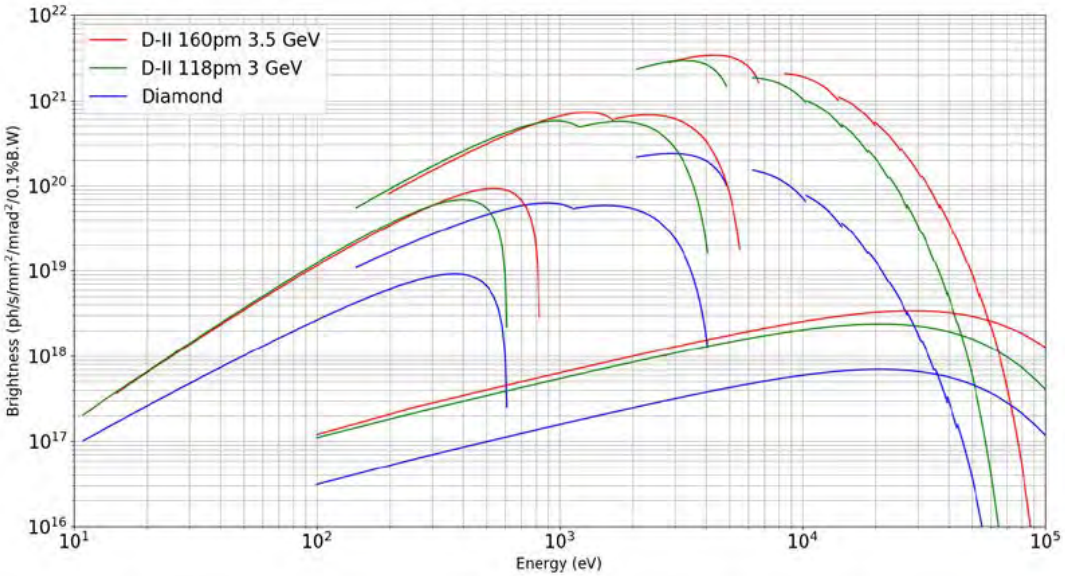

Figure 1-2 : Brightness for a set of selected sources at Diamond (blue curves), Diamond-II at 3 GeV (green curves) and Diamond-II at 3.5 GeV (red curves). In the UV regime, soft X-ray regime and hard X-ray, the brightness curves are shown respectively for the I05, I21, the future CPMU 15.6 mm period (to be installed on I11 and VMXm), and for the superconducting wiggler on I12 (JEEP). All calculations have been made with Spectra 9 using the Wigner function. A phase error of 3° for the undulators has been taken into account analytically.

Coherent Fraction

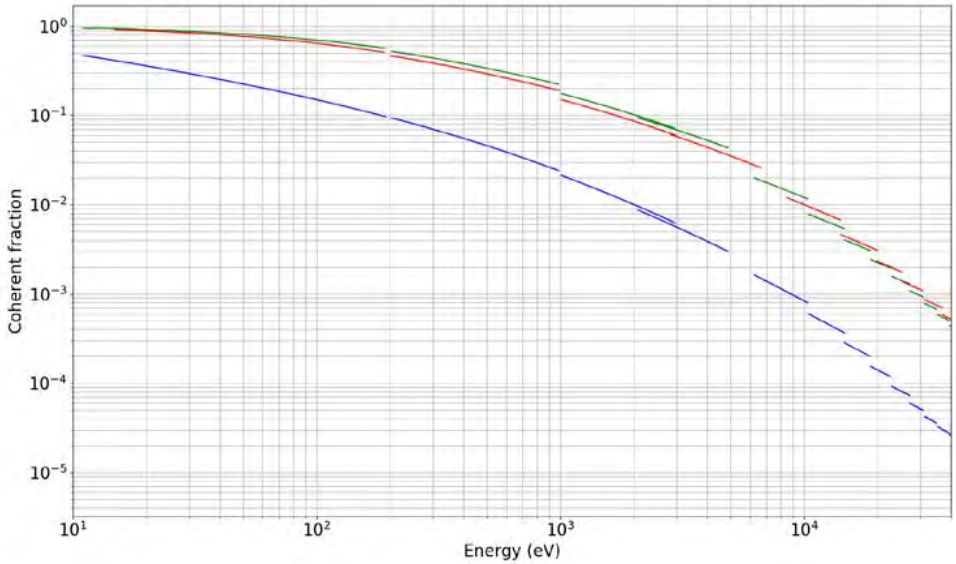

Figure 1-3 : Coherent fraction in the horizontal direction as a function of Energy for Diamond (blue), Diamond-II at 3 GeV (green) and Diamond-II at 3.5 GeV (red). All curves have been produced with Spectra using the Wigner function and approximating the coherent fraction as the ratio between the Brightness and the Brightness calculated in the limit of zero emittance and zero energy spread.

Compromise to achieve the science at Diamond

The Diamond-II lattice has therefore been designed with the lowest possible emittance with the constraints of:

- doubling the number of straight sections by including a mid-straight at the centre of each cell
- increasing the energy to 3.5 GeV
- maintaining certain minimum straight section lengths
- making minimal changes in position and angle of source points
- preserving off-axis injection with top-up.

Photon energy (keV)	Gain in brightness Diamond-II at 3 GeV (118pm)	Gain in brightness Diamond-II at 3.5 GeV (160pm)
1	x 10	x 8
25	x 18	x 49
40	x 17	x 79

Table 1: *Gain in brightness with Diamond-II at 3 or 3.5 GeV, calculated using the Wigner formulation.*

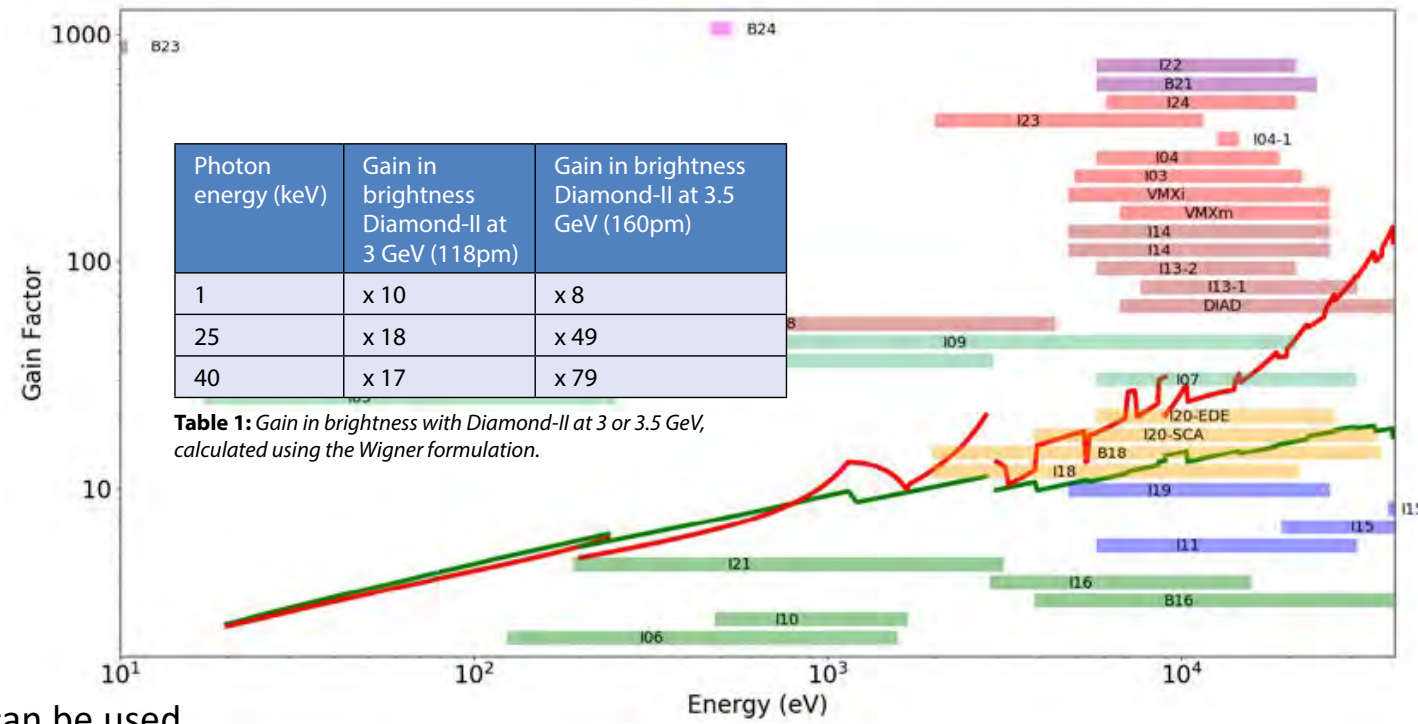

160 pm.rad
3.5GeV

118 pm.rad
3.0GeV

Figure 1-4: Gain in spectral brightness for a set of selected undulator sources for Diamond-II at 3 GeV, 118 pm emittance (green curves) and Diamond-II at 3.5 GeV, 160 pm emittance (red curves). In the UV regime, soft X-ray regime and hard X-ray, the brightness curves are shown respectively for the I05, I21, and the future CPMU 15.6 mm period (to be installed on I11 and VMXm). The photon energy ranges used for all current Diamond beamlines are represented by horizontal bars. Beamlines B22 (IR) and I12 (high-energy engineering) energies are outside of the range of this graph.

8 new mid-straights can be used

Create one new long straight

Preserve all bending magnet beamlines and offer ID upgrades

diamond

Diamond-II | Advancing Science

The Coherent Soft X-ray Imaging and Diffraction beamline CSXID

David Burn

Diamond-II | Advancing Science

CSXID experimental techniques

Ptychography

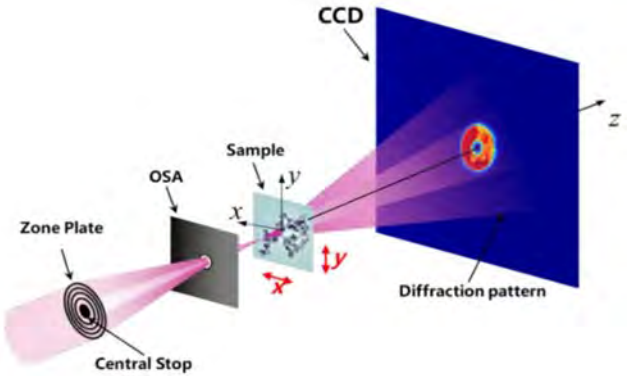

Holography

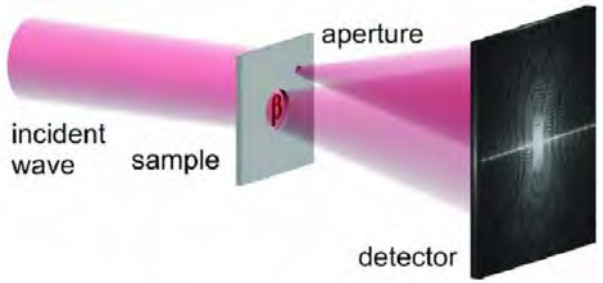

Bragg CDI

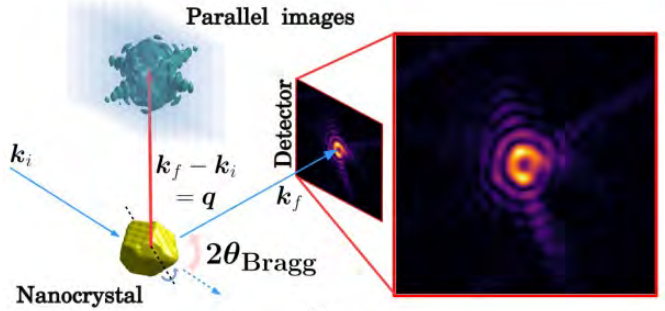

Phys. Rev. A 99, 053838 (2019)

Tomography

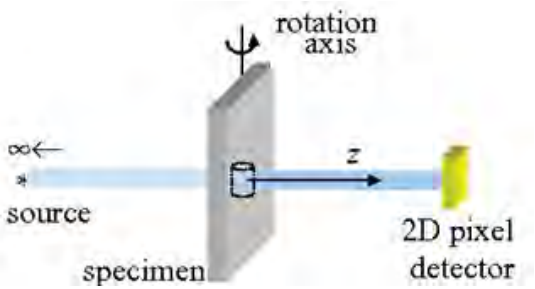

Laminography

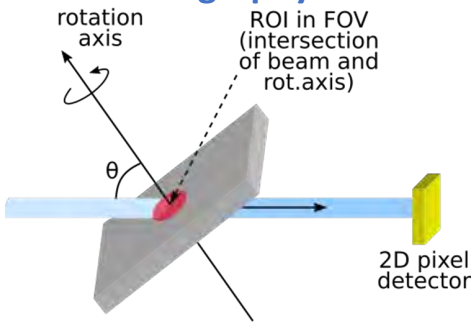

Magnetic contrast

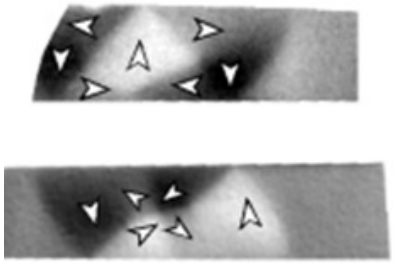

M. Klaui, et.al. Appl. Phys. Lett. 88 (2006) 232507.

Chemical contrast

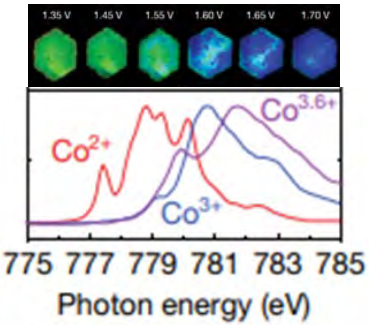

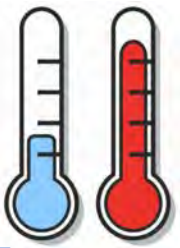

Temperature

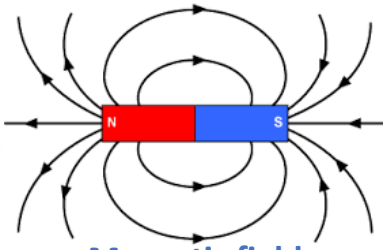

Magnetic field

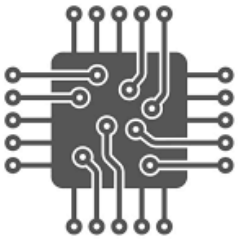

Electrical connections

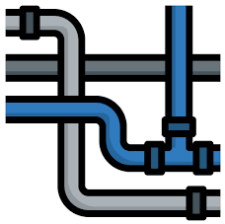

Liquid and gas delivery

Time resolution

Environment development

Spectroscopy WIthin Fast Timescales: beamline SWIFT

Giannantonio Cibin

Diamond-II | Advancing Science

SWIFT: Science drivers

Nanoparticle chemistry

Time resolution

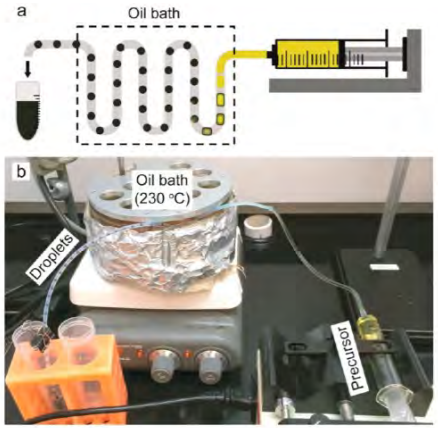

Figure 1. (a) Schematic illustration of the fluidic device used for generating droplets in situ, followed by the formation of Pt–Ni octahedral nanocrystals within each droplet. (b) Photograph showing the formation of droplets in a PTFE tube during the continuous pumping of a precursor solution containing $W(CO)_6$ at a concentration of 2.0 mg mL^{-1}.

Metalloenzymes

Flux And time resolution

Radiation damage

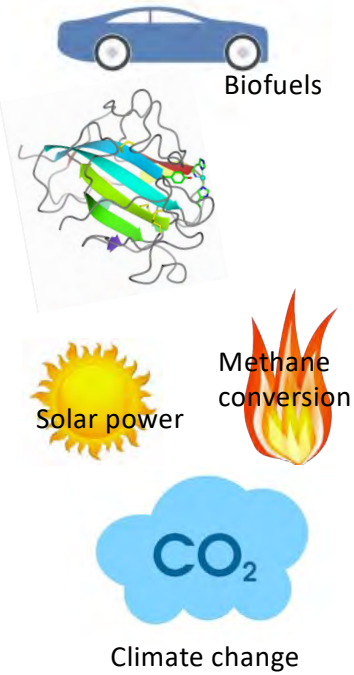

Catalysis:

Mapping, Spectroscopies

Time resolution

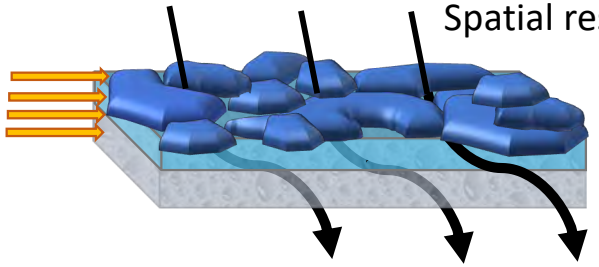

Energy:

spatial and time resolution in batteries

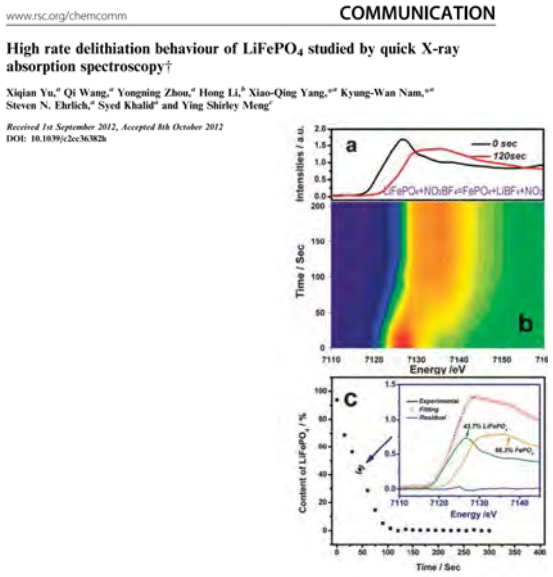

Environment and Earth sciences

Spatial resolution, radiation damage control

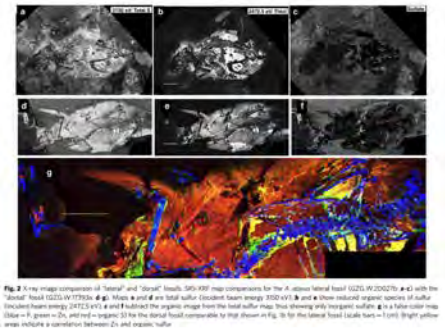

Courtesy of Giannantonio Cibin

Source: 13-pole wiggler in a mid-straight section

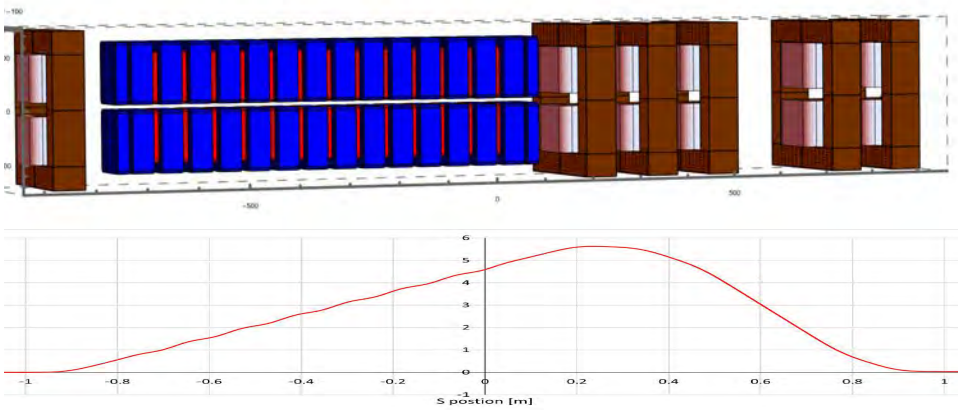

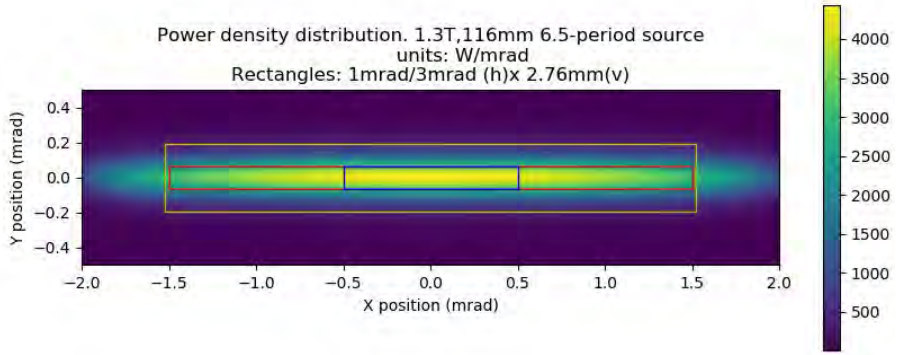

Multi-pole wiggler - 3.2 kW total power
Source is off-axis to the nominal trajectory

Will give 10-15 times more photons than B18

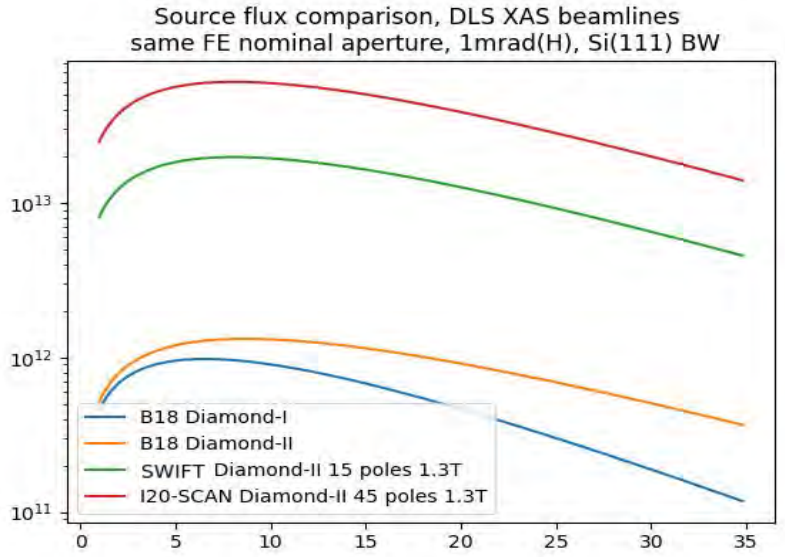

diamond

Diamond-II | Advancing Science

QUICK-EXAFS Monochromator

Monochromators: High power load, LN cooled

- **Quick-EXAFS**, fast-scanning DCM (50Hz, 4-35 keV)
  - Channel-cut, direct-drive, direct cooling
- **Continuous-scanning**, fixed exit (‘conventional’)

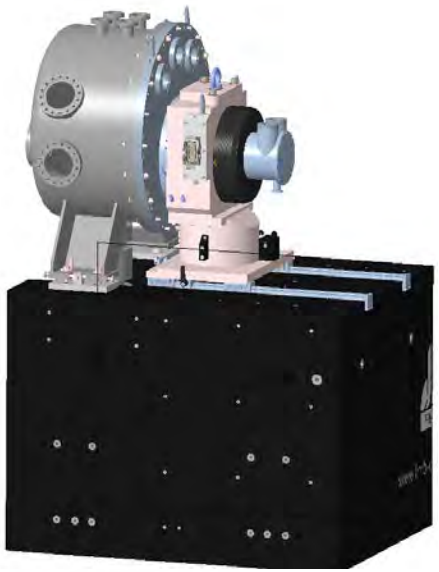

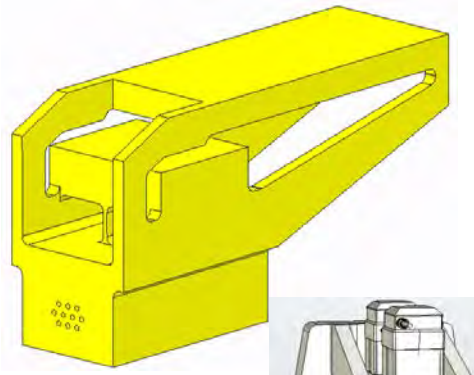

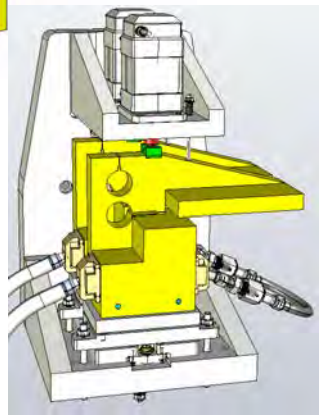

Preliminary studies quite advanced:

Challenges are thermal load and alignment accuracy under high dynamical conditions

Complex crystal design, direct LN2 cooling
LN2 joints under vibrations

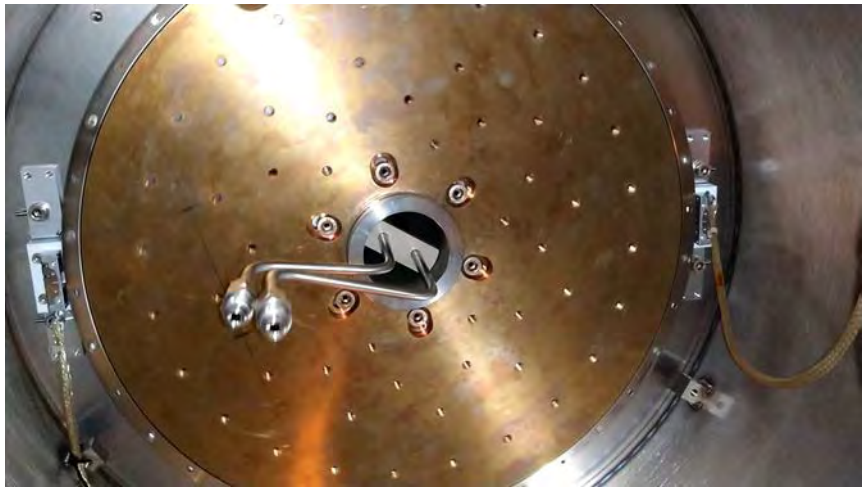

diamond

Courtesy of Giannantonio Cibin

Endstations

Experimental Hutch 1: bulk

- High flux
- Operando studies, dilute systems
- Beam size: 100 x 100 um

Experimental Hutch2: microfocus

- Beam size: 20 x 20 um
- Sample chemical mapping, tomography

Operando sample environments

- High temperature
- Gas flow reaction cells
- Liquid flow reaction cells
- Electrochemistry

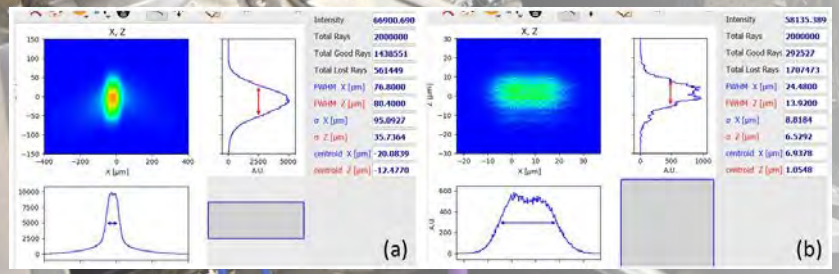

Courtesy of Giannantonio Cibin

diamond

Diamond-II | Advancing Science

Endstations: Ancillary instrumentation

Again, will expand on the experience from the present Spectroscopy beamlines

To characterise the sample conditions during operando experiments

- **Mass Spectrometers**
- **Potentiostats**
- **UV-VIS spectrometers**
- **FTIR, Raman**

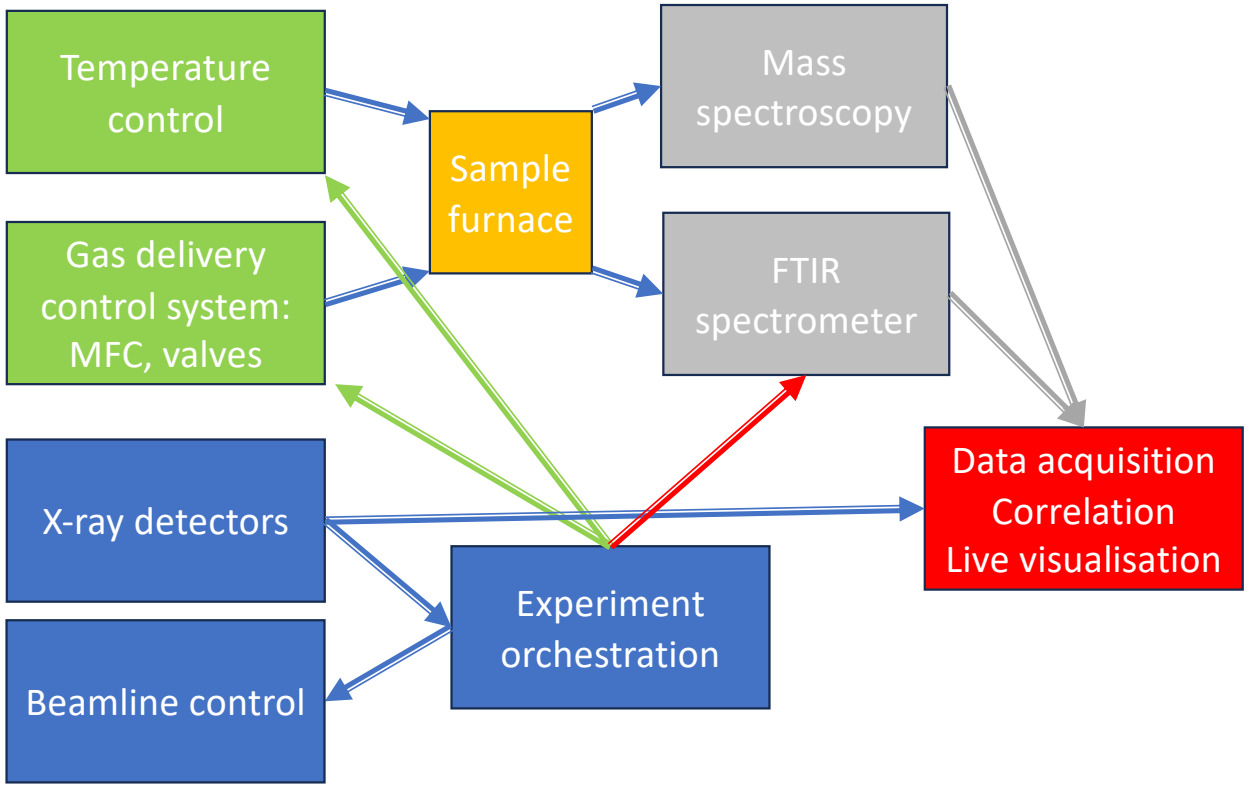

- **Essential is development of software interfaces - EPICS, BlueSky**
  - Need: correlate time-resolved conventional instrumentation and beamline data
  - Control integrated with data acquisition system
  - Intake of time-resolved data for live processing

Courtesy of Giannantonio Cibin

Opportunities and Challenges

What we should consider in the theory

Study 1: Experimental setup and method

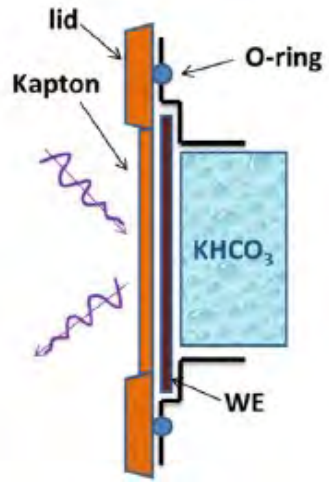

Experimental method

- CA measurements at fixed potential: OCP, -0.5V,-1V, -1.5V, -2V held for 30 minutes EXAFS spectra acquired every 3minutes.
- CV measurements were conducted on the electrocatalysts in the potential interval 0/-2 V (vs Ag/AgCl) at a scan rate of 10 mVs-1. XANES spectra acquired every 20s

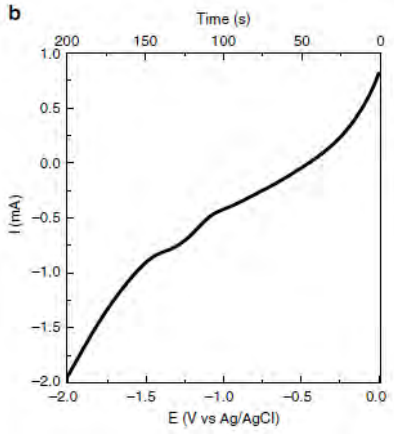

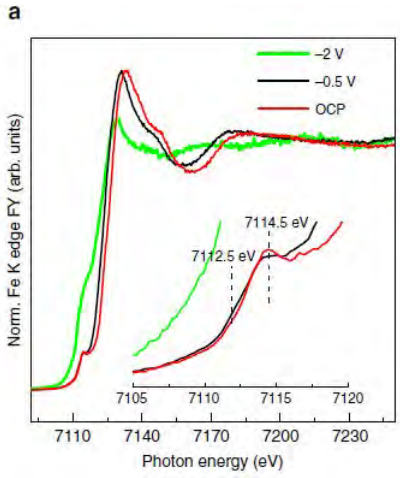

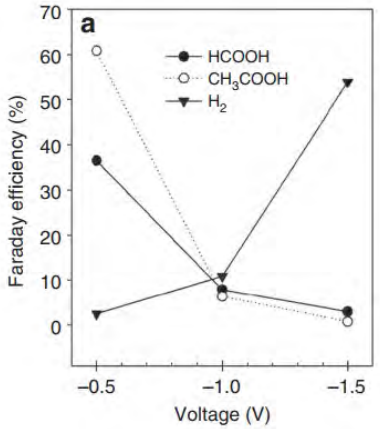

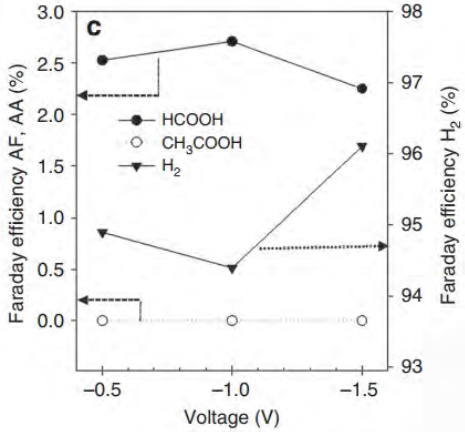

Courtesy of Diego Gianolio

Study 1: data analysis

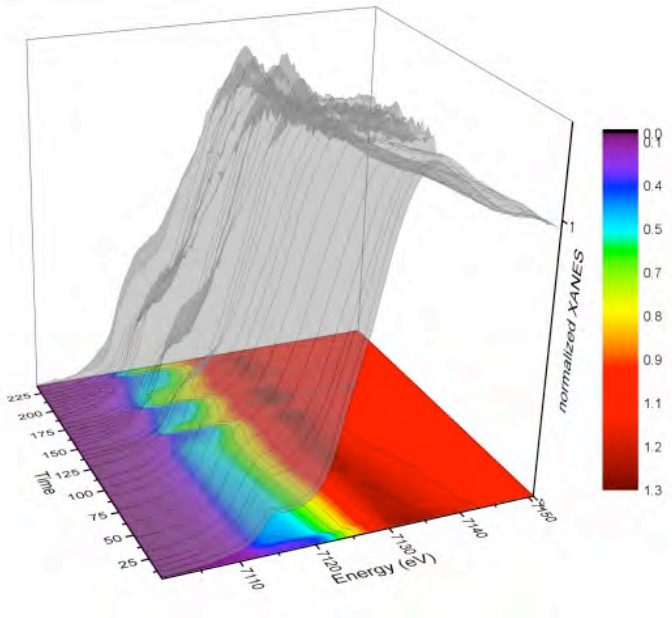

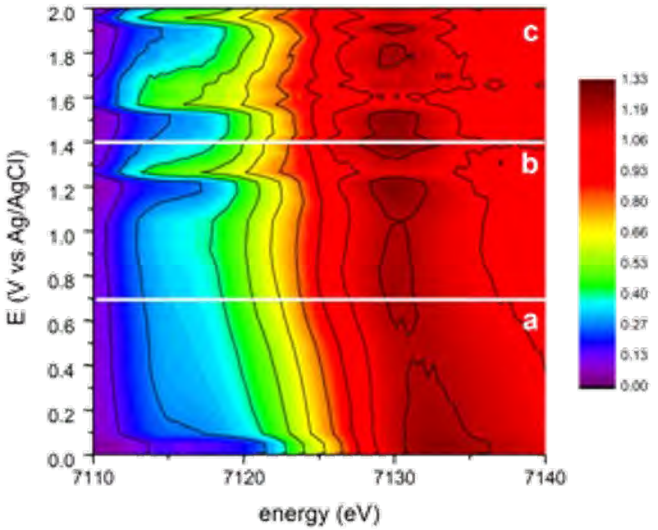

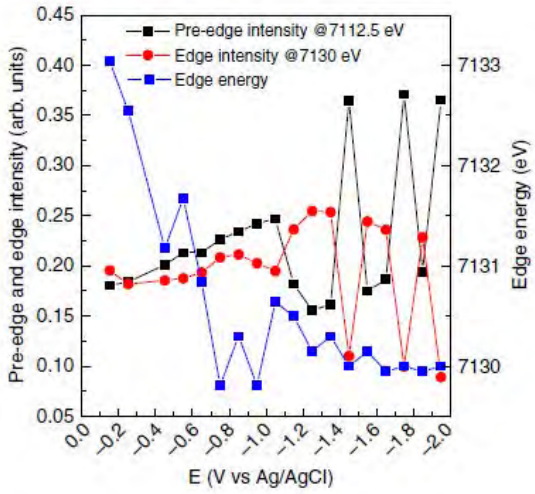

We can distinguish 3 potentials windows where catalyst have different properties

a) -0.15V (OCP) to -0.55V prevalent CO2RR reaction

b) -0.65V to -1.25V HER becomes dominant

c) -1.45V to -1.95V highest HER rate but catalyst unstable

Courtesy of Diego Gianolio

Study 1: Conclusions

Outstanding CO2RR FE and high selectivity derive from the synergistic effect between the carbon

The potential at which the Fe(II) sites are formed dictates the potential for

Should go beyond valence state, bond lengths. Details of are important, more useful

Synthetic strategies for improved catalysts must aim to maximize the stabilization of small Fh-FeOOH clusters

have a double effect: coordinate CO2-species, promoting C-C coupling stabilize Fe sites inhibiting HER

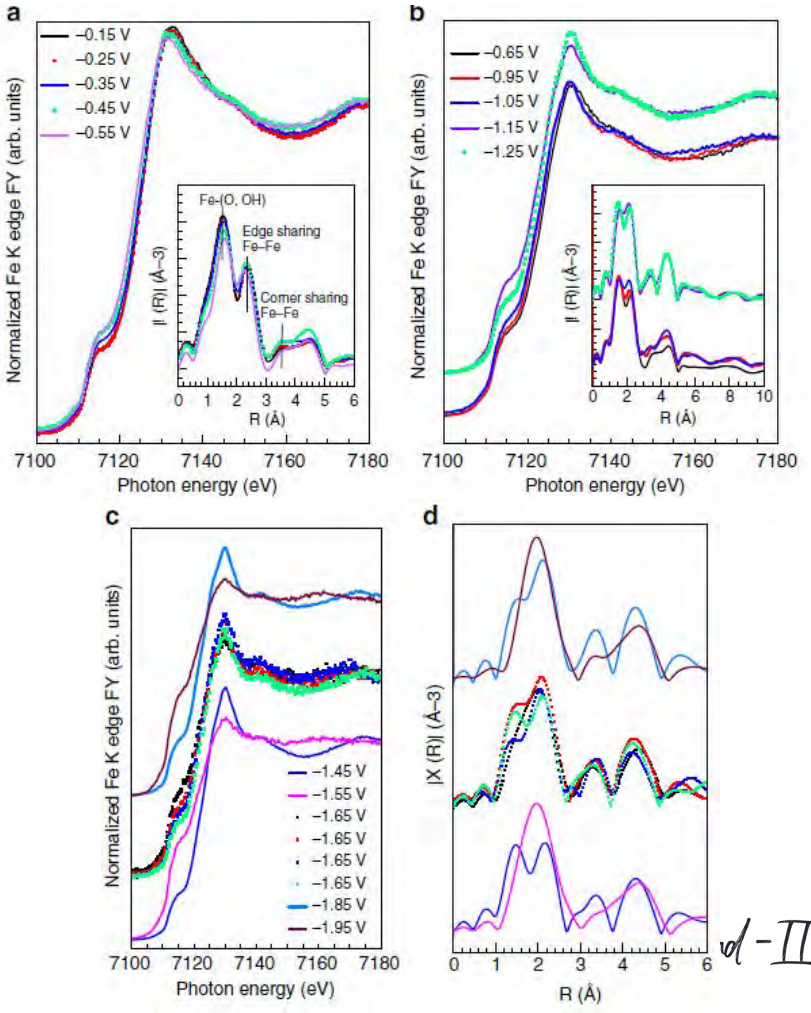

Region a)

- Shift in edge energy highlight formation of Fe(II) sites
- EXAFS shift of Fe-O to higher distances is in agreement with the interpretation of XANES

Region b)

- The slight increase of the pre-edge at 7112.5 eV indicates the formation of Fe(0).
- EXAFS still measure the presence of Fe-O bonds

Region c)

- formation of intermediate Fe-hydride species from OH dissociation.
- adsorbed H+ are discharged as H2, leaving Fe(0) behind.

diamond

Courtesy of Diego Gianolio

Angewandte International Edition Chemie
GDCh A Journal of the German Chemical Society

Research Article | Open Access

The Electrophilicity of Surface Carbon Species in the Redox Reactions of CuO-CeO_2 Catalysts

Liqun Kang, Dr. Bolun Wang, Dr. Andreas T. Güntner, Siyuan Xu, Xuhao Wan, Yiyun Liu, Sushila Marlow, Yifei Ren, Dr. Diego Gianolio, Dr. Chiu C. Tang, Dr. Vadim Murzin ... See all authors

First published: 17 March 2021 | https://doi.org/10.1002/anie.202102570 | Citations: 4

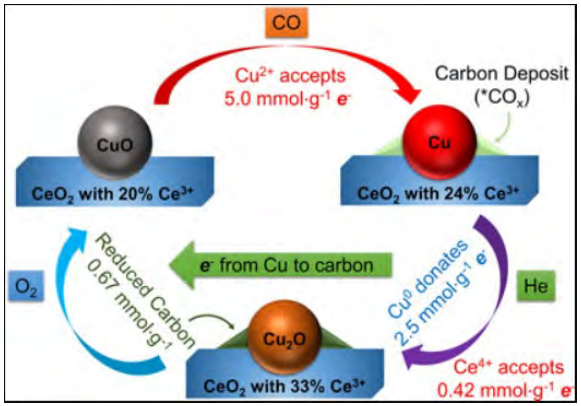

Prof. R. Wang UCL, procurement and commissioning of Pilatus detector in B18

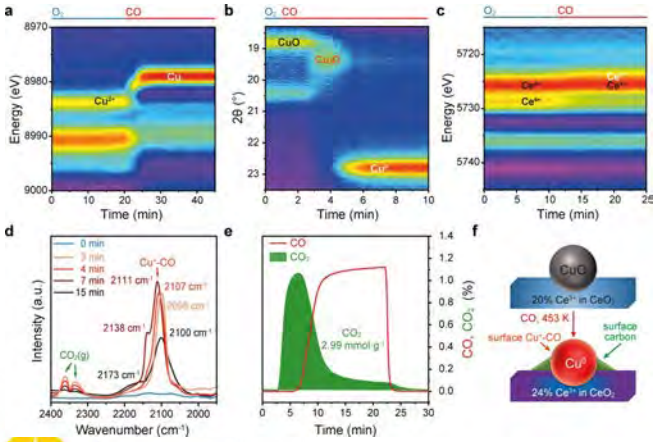

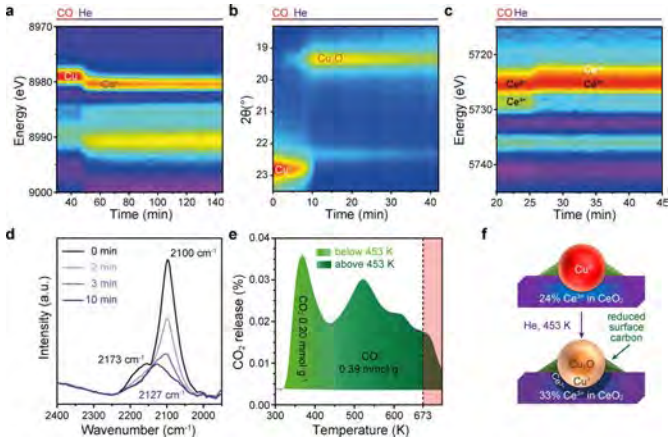

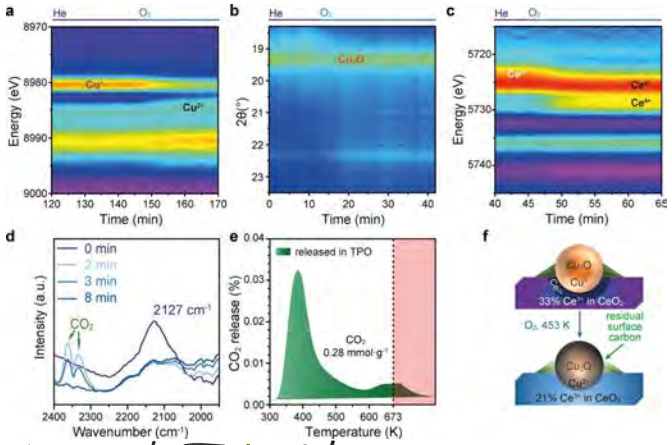

diamond

Courtesy of Diego Gianolio

Diamond-II | Advancing Science

Li ion batteries charge/discharge mechanism

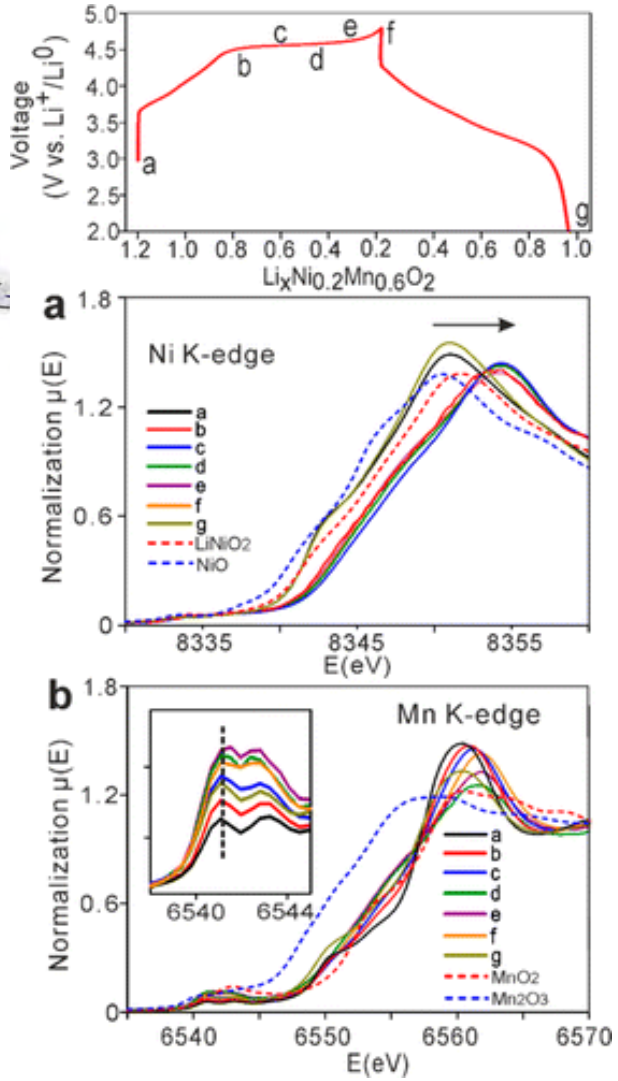

nature chemistry ARTICLES
PUBLISHED ONLINE: 21 MARCH 2016 | DOI: 10.1038/NCHEM.2471

Charge-compensation in 3*d*-transition-metal-oxide intercalation cathodes through the generation of localized electron holes on oxygen

Kun Luo[†], Matthew R. Roberts[†], Rong Hao[1], Niccoló Guerrini[1], David M. Pickup[2], Yi-Sheng Liu[3], Kristina Edström[4], Jinghua Guo[3], Alan V. Chadwick[2], Laurent C. Duda[5] and Peter G. Bruce[1]*

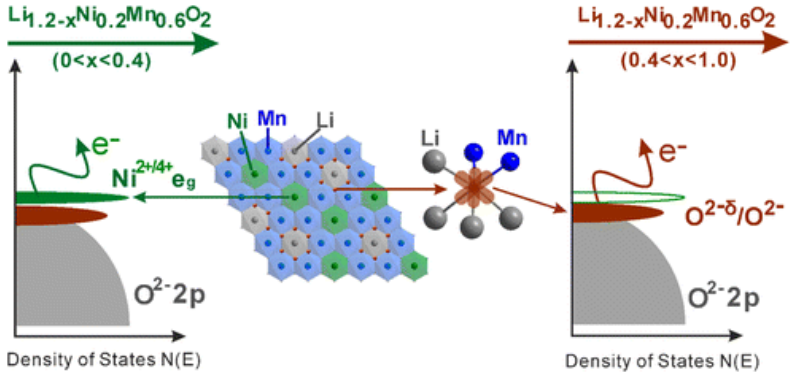

Energy materials

diamond

Courtesy of Diego Gianolio

Diamond-II | Advancing Science

Alanine on Ni{111}

Angle-resolved NEXAFS

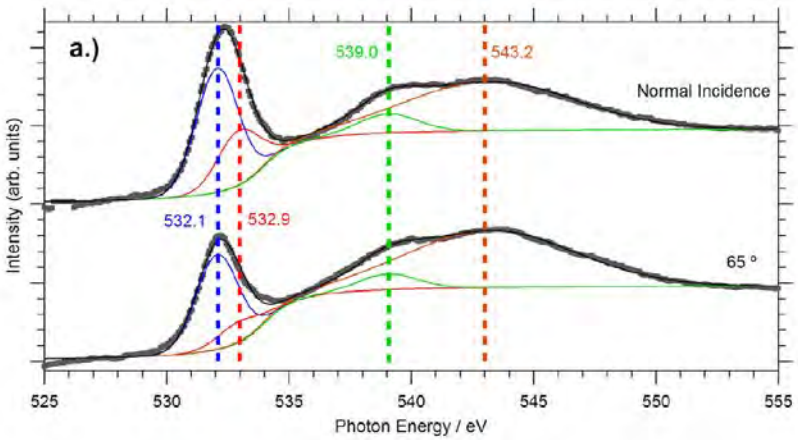

- DFT: VASP (J. Ontaneda, R. Grau-Cresopo)
- Experiment: Ni{111} @ 300 K; Nicklin et al. J. Phys. Chem. C 119 (2015) 26566 .

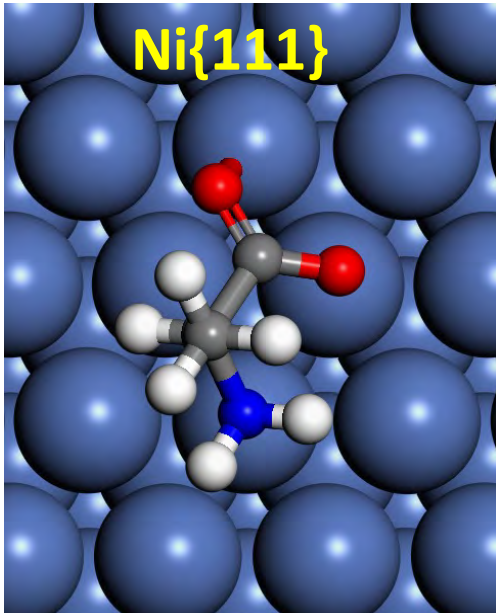

O1s XPS

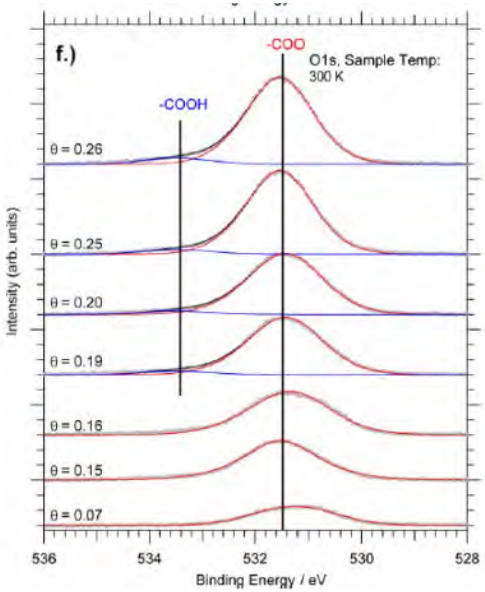

- Experimental O 1s BE shifts well reproduced.
- Angle OCO vs surface significantly different from experimental values (60°) obtained using gas-phase orbital symmetry.
- Need better modelling of NEXAFS / XAS

Courtesy of Georg Held

∢ OCO DFT	23.0°
∢ OCO NEXAFS	60°
ΔBE O 1s DFT	0.01 eV
ΔBE O 1s XPS	~ 0 eV

Opportunities

- 1) Intermediate states in reactions: full chemistry and not the ionic formal bond picture: not the bulk sample, the real one with full electrons / protons transfers with environment

More complex spectroscopies

HERFD, XES and RIXS

ZnO HERFD-XAS (Zn *K*-edge)

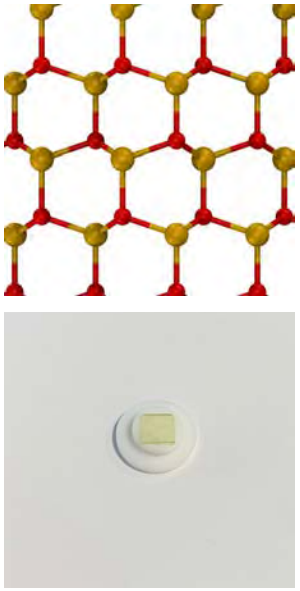

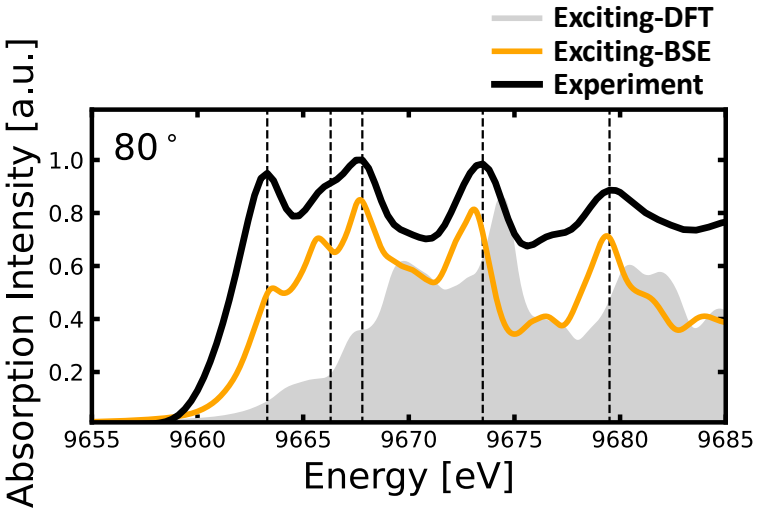

Angularly-dependent HERFD-XAS

Polarization parallel (90°) - perpendicular (0°) to c-axis.

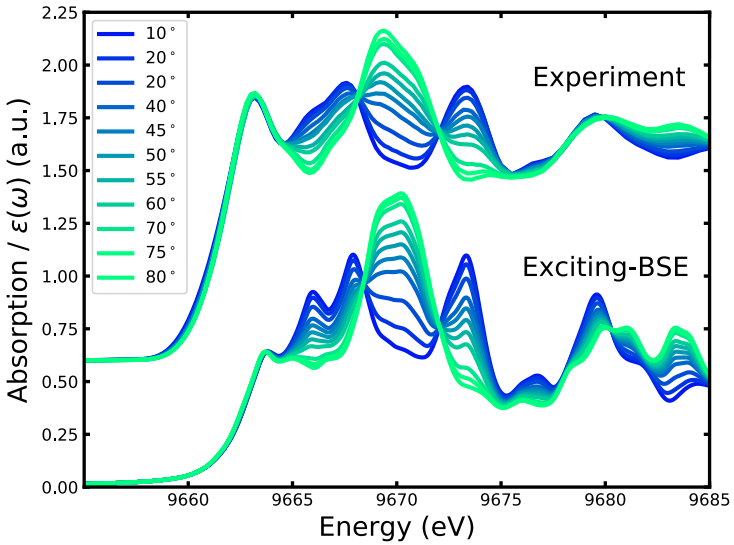

- Single Crystal HERFD-XANES spectra measured on I20-Scanning Beamline at Diamond Light Source
- Simulations Carried out using Exciting Code[1] on Archer2 (Access provided by HPC-CONEXS).
- **Beyond-DFT** methods based on the **Bethe-Salpeter Equation** formalism provide significantly better agreement with the experiment.
- BSE simulations of the XANES spectrum fully account for changes associated with polarization of incident beam

[1]J. Phys.: Condens. Matter 26, 363202 (2014)., Phys. Rev. Res. 2, 042003 (2020)., Phys. Chem. Chem. Phys. 24, 17439 (2022).

diamond

Courtesy of Joshua Elliott

Diamond-II | Advancing Science

Resonant Inelastic X-ray Scattering: photon-in, photon-out technique

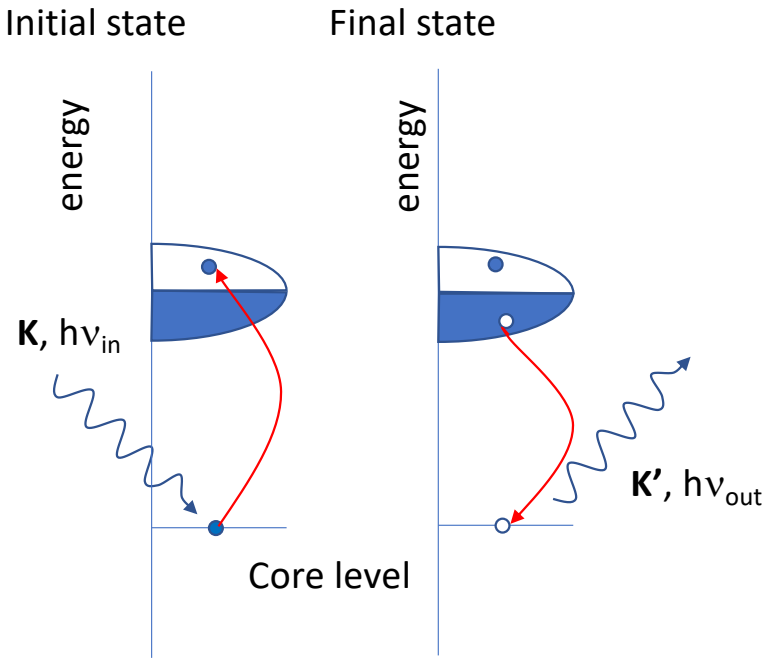

Probing occupied states

$|\mathbf{0}\rangle$ - **Ground-State**
$|I\rangle$ - **Intermediate State (Core excitation)**
$|F\rangle$ - **Final State (Scattering product)**

Double Differential Cross Section

Heisenberg-Krammers relationship

$$\frac{d^2\sigma}{d\Omega d\omega} \propto \sum_F \left| \sum_I \frac{\langle F|\hat{T}^\dagger(\mathbf{e}_2)|I\rangle\langle I|\hat{T}(\mathbf{e}_1)|\mathbf{0}\rangle}{\omega - E_I - i\eta_I} \right|^2 \times \delta(E_F - E_0 + \omega' - \omega)$$

Courtesy of Joshua Elliott

diamond

Diamond-II | Advancing Science

ZnO RIXS (Zn 1*s*2*p*-plane)

- Angularly-dependent RIXS maps of the Zn 1*s*2*p*-plane also measured on I20-Scanning Beamline at Diamond Light Source
- Simulated RIXS maps correlate DFT ground state $|\mathbf{0}\rangle$, BSE K-edge excited states $|I\rangle$ and BSE L-edge excited states $|F\rangle$.
- Fully converged simulations require **58k** BSE transitions at the *K*-edge and **121k** BSE transitions at the *L*-edge.
- BSE RIXS maps reproduce features in experimental RIXS maps, and allows us to identify the transitions responsible through analysis of excitonic states.

Elliott, Hayama, Diaz-Moreno – *In Preparation (2024)*

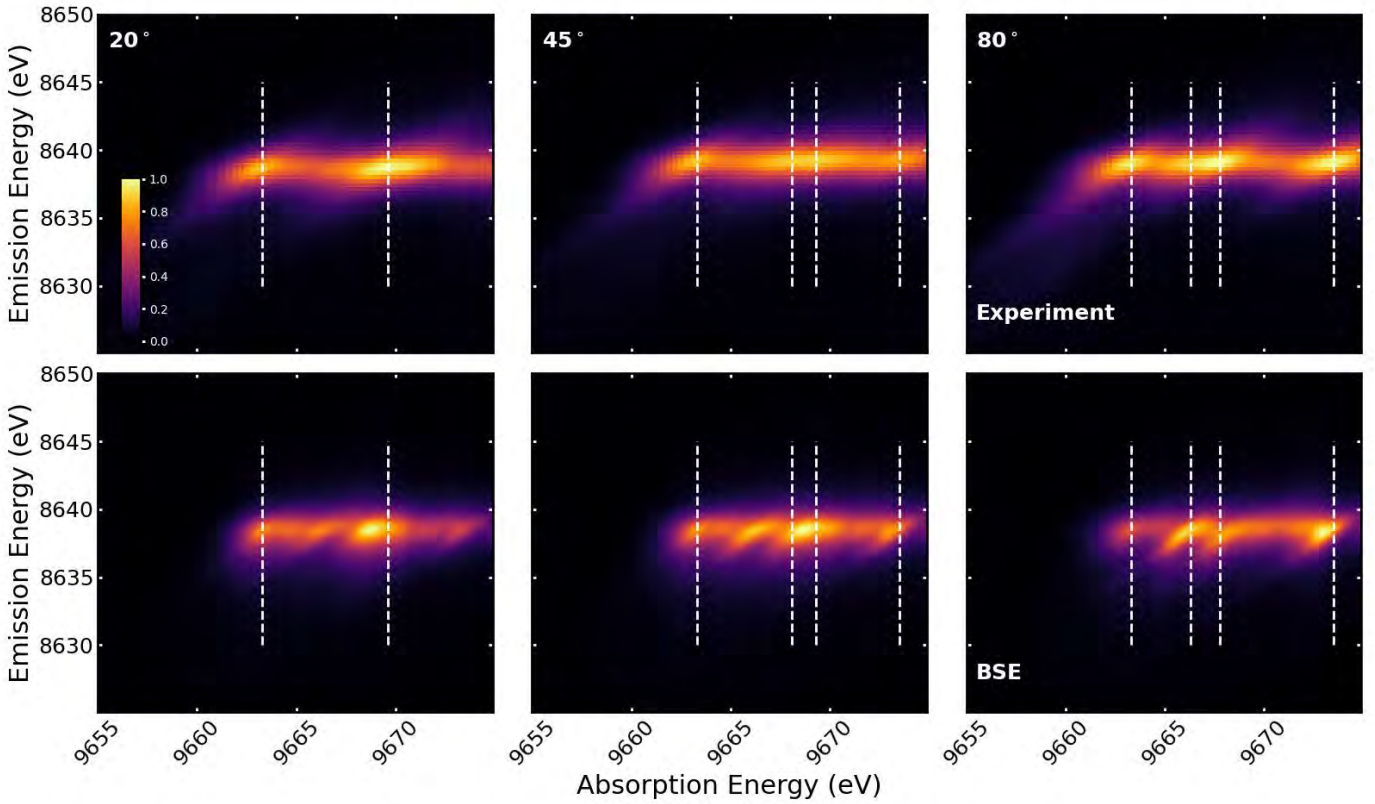

Courtesy of Joshua Elliott

Article

Chiral phonons in quartz probed by X-rays

https://doi.org/10.1038/s41586-023-06016-5

Received: 20 January 2023

Accepted: 27 March 2023

Hiroki Ueda[1,2]✉, Mirian García-Fernández[3], Stefano Agrestini[3], Carl P. Romao[4], Jeroen van den Brink[5,6], Nicola A. Spaldin[4], Ke-Jin Zhou[3] & Urs Staub[1]✉

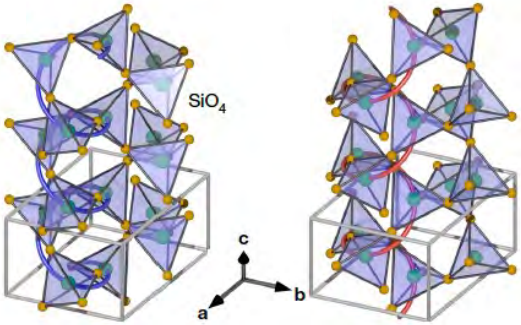

Quartz has a chiral structure leading to chiral phonons arising from the light-matter interaction.

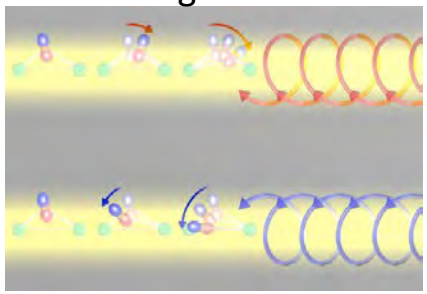

Chiral structures possess chiral phonons – *i.e.* rotational atomic motion perpendicular to the phonon propagation direction.

Optical probes, which probe the zone centre, are not sensitive to such vibrational modes.

Resonant Inelastic X-ray Scattering (RIXS) at the O K-edge (534eV) was used to observe chiral phonons for the first time.

H. Ueda *et et al.*, Nature **618**, 946 (2023)

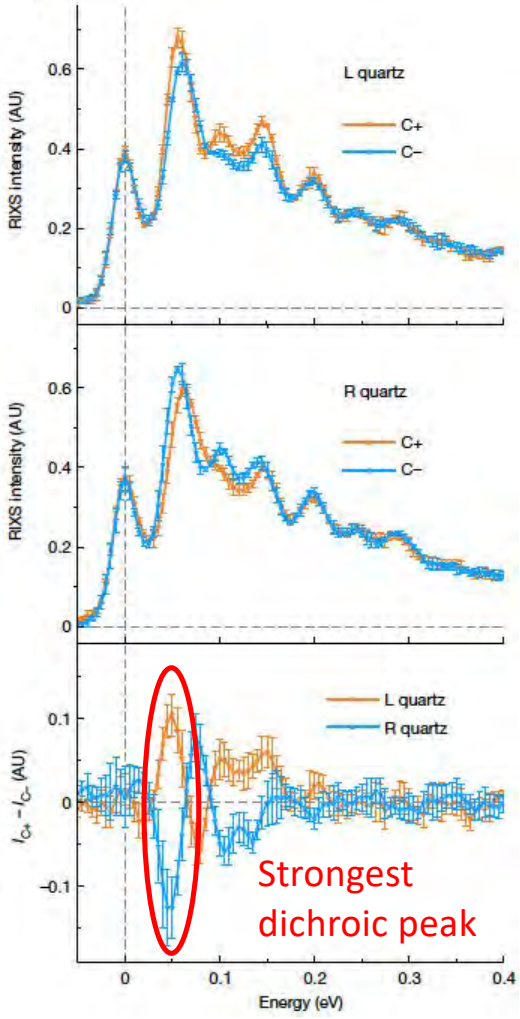

diamond

Courtesy of Sarnjeet Dhesi and Ke-Jin Zhou

Diamond-II | Advancing Science

DFT to identify phonon modes, dispersion, chirality and magnetic moments

Phonon chirality

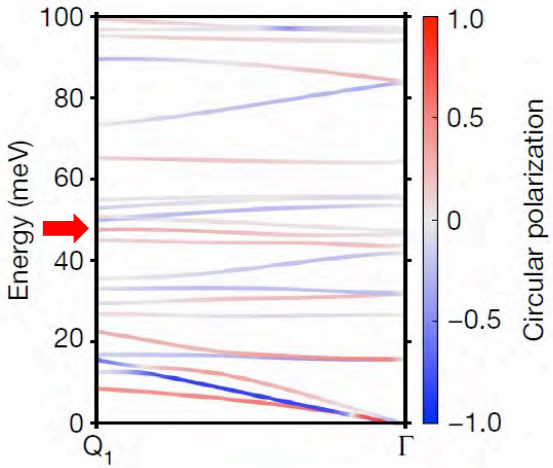

Light interaction strength

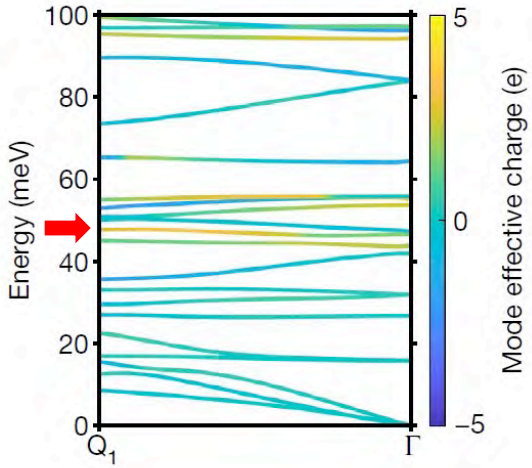

Phonon magnetic moment

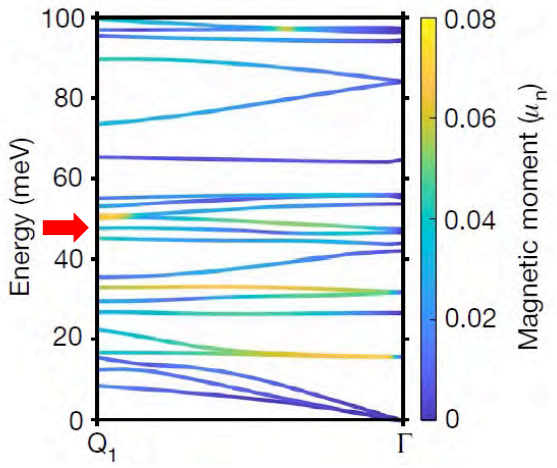

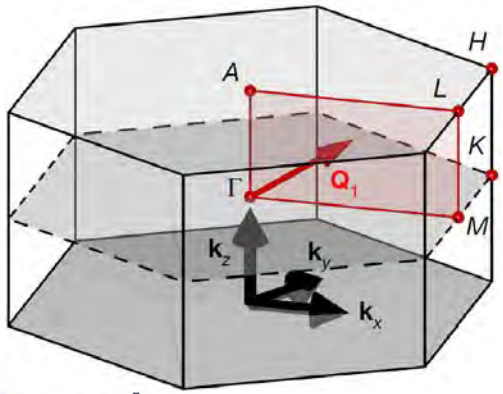

RIXS was measured at a low-symmetry point (Q_1) in the BZ and DFT used to calculate the phonon dispersion along ΓQ_1

DFT demonstrates that the strongest dichroic peak in the RIXS spectrum at ~50meV arises from modes (red arrows) with a large chirality and strong interaction with the light. DFT can also indicate the magnetic moment of the phonon mode.

Courtesy of Sarnjeet Dhesi and Ke-Jin Zhou

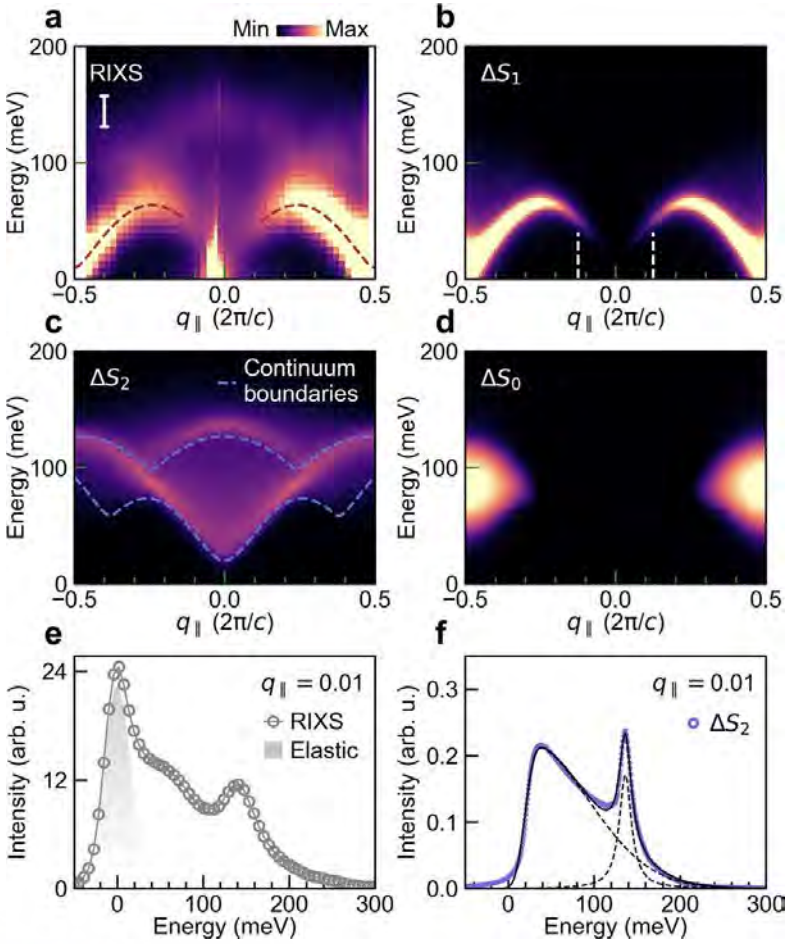

ARTICLE

https://doi.org/10.1038/s41467-022-30065-5 OPEN

Check for updates

Quadrupolar magnetic excitations in an isotropic spin-1 antiferromagnet

A. Nag[1,7✉], A. Nocera[2,3✉], S. Agrestini[1], M. Garcia-Fernandez[1], A. C. Walters[1], Sang-Wook Cheong[4], S. Johnston[5,6✉] & Ke-Jin Zhou[1✉]

Collective quadrupolar magnons ($\Delta S = 2$) were revealed for the first time by RIXS in a one-dimensional S = 1 quantum spin-chain antiferromagnet, Y_2BaNiO_5.

Inelastic neutron scattering, is only sensitive to collective dipolar magnons ($\Delta S = 1$) and is insensitive to higher-order excitations.

Density matrix normalization group (DMRG) is well known for understanding the low-energy physics of the spin-chain systems with various spin model.

Here, DMRG was applied to compute the dynamical spin correlation functions: $S_0(q, \omega)$, $S_1(q, \omega)$, $S_2(q, \omega)$ giving information about $\Delta S_{tot} = 0$, $\Delta S_{tot} = 1$, $\Delta S_{tot} = 2$ excitations respectively (shown in the left figures).

A. Nag *et al.*, Nature Communications **13**, 2327 (2022)

Courtesy of Sarnjeet Dhesi and Ke-Jin Zhou

LETTER

https://doi.org/10.1038/s41586-018-0648-3

Three-dimensional collective charge excitations in electron-doped copper oxide superconductors

M. Hepting[1], L. Chaix[1,9], E. W. Huang[1,2], R. Fumagalli[3], Y. Y. Peng[3,10], B. Moritz[1], K. Kummer[4], N. B. Brookes[4], W. C. Lee[5], M. Hashimoto[6], T. Sarkar[7], J.-F. He[1,11], C. R. Rotundu[1], Y. S. Lee[1], R. L. Greene[7], L. Braicovich[3,4], G. Ghiringhelli[3,8], Z. X. Shen[1]*, T. P. Devereaux[1]* & W. S. Lee[1]*

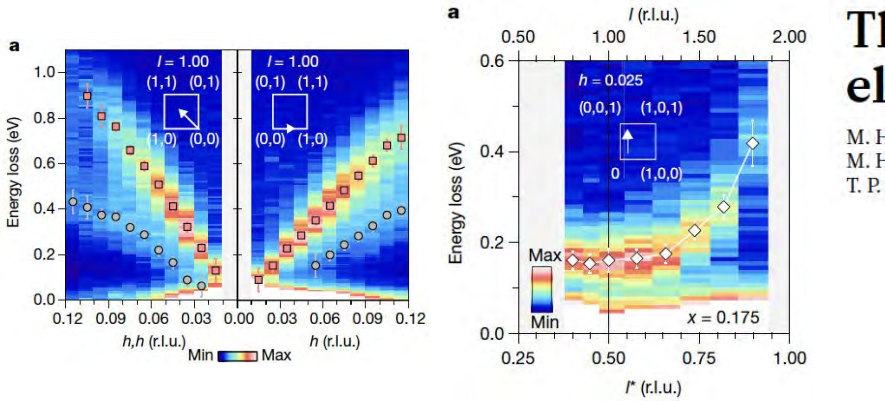

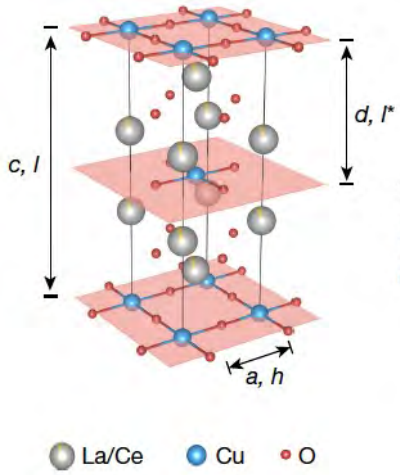

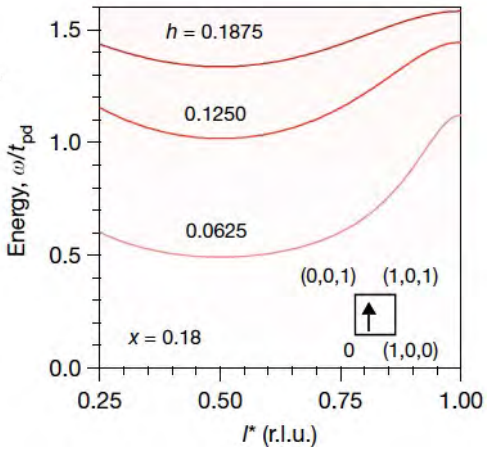

Three-dimensional collective charge excitations (plasmons) have long been predicted, and were recently discovered by RIXS in cuprates owing to the inter-layer long-range Coulombic interaction.

The Determinant Quantum Monte Carlo (DQMC) method was used to compute the dynamical charge susceptibility in the 2D Hubbard model for doped cuprates and incorporate the three-dimensional Coulomb interactions using a random-phase-approximation formalism (RPA).

M. Hepting *et al.*, Nature **563**, 374 (2018)

diamond

Courtesy of Sarnjeet Dhesi and Ke-Jin Zhou

The Energy Loss Spectrum

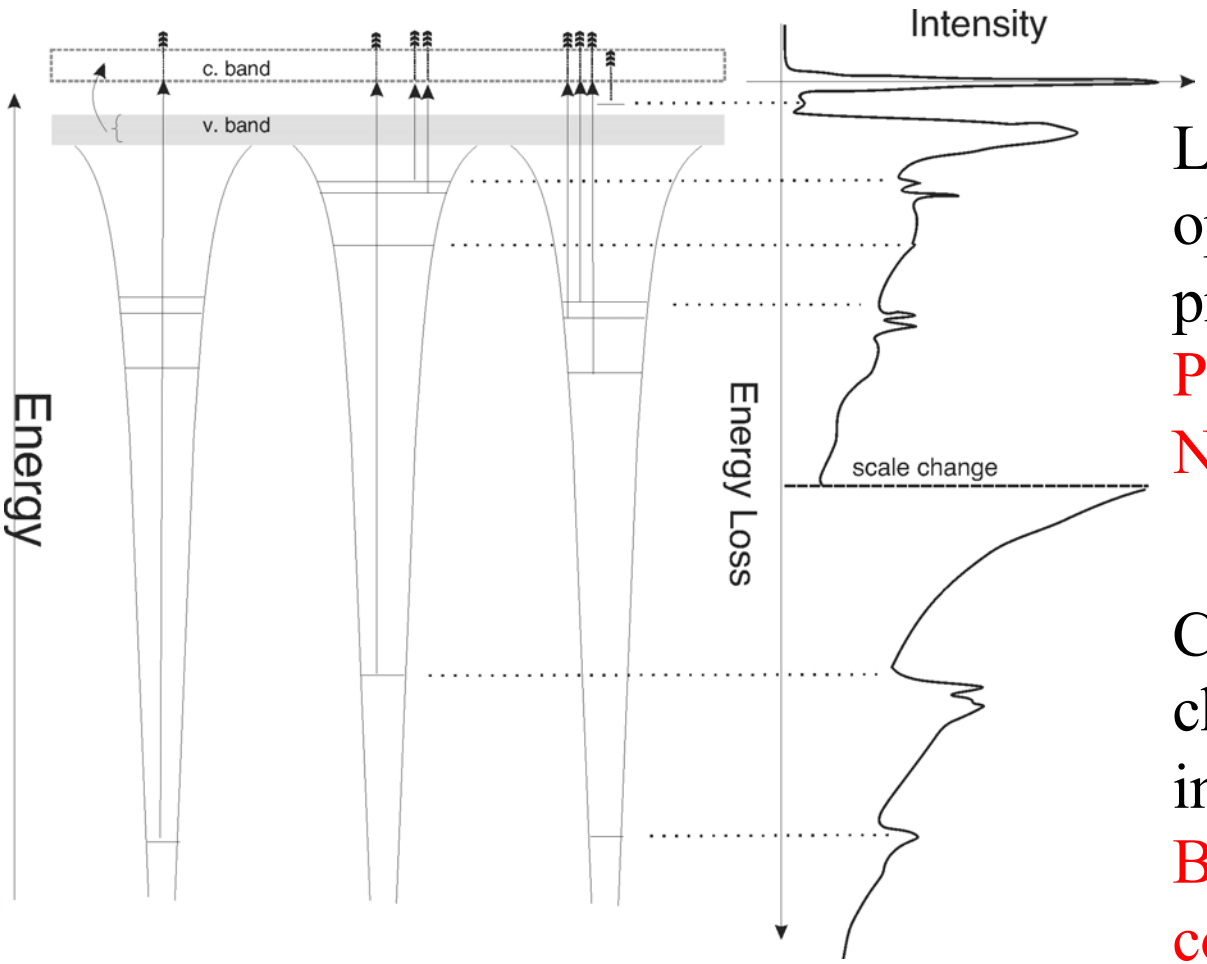

Low-loss: optical properties Plasmonics, Nanoantennas

Core-loss: chemical information Bonding, composition

G. Botton, MRS Bulletin, Review article, Special issue, Jan 2012

Energy Loss Near Edge Structures

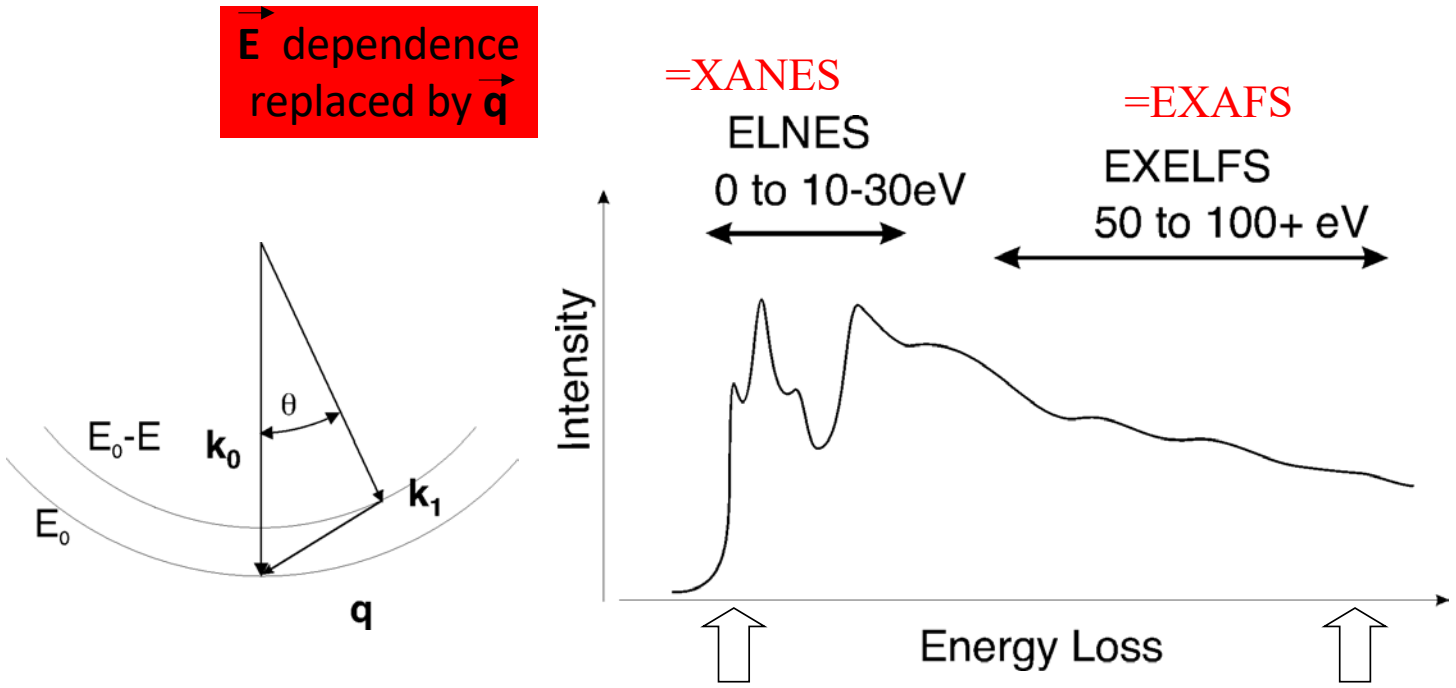

$$\varepsilon_n = \int \psi_n^* \sum_j \exp(iq\cdot r)\psi_0 d\tau = \left\langle \psi_n \left| \sum_j \exp(iq\cdot r) \right| \psi_0 \right\rangle$$

Botton, in Encyclopedia "Science of Microscopy", Radtke & Botton, in "STEM"

Probing unoccupied states

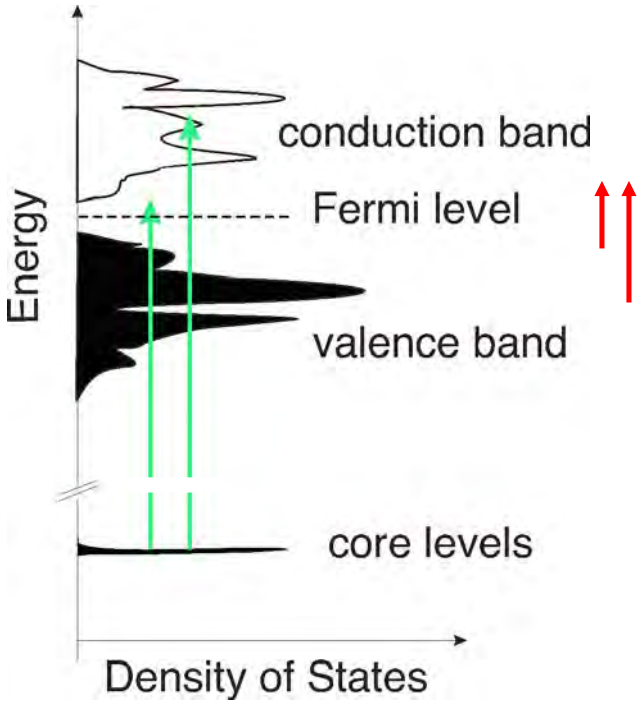

Optical spectroscopy

(with core-hole effects as in XAS)

$$\frac{d^2\sigma}{d\Omega dE} \propto \left(\frac{1}{\theta^2+\theta_E^2}\right)\mathrm{Im}\left[-1/\varepsilon(q,E)\right]$$

$$\mathrm{Im}(-1/\varepsilon) = \varepsilon_2/\left(\varepsilon_1^2+\varepsilon_2^2\right) = \varepsilon_2$$

At high energy (ε1->1) (screening small)

$\varepsilon_2 << \varepsilon_1$

$$\frac{d^2\sigma}{d\Omega dE} \propto \sum_{i,f}\left|\langle\psi_f|\exp(i\mathbf{q}\cdot\mathbf{r})|\psi_i\rangle\right|^2\delta(E-E_f+E_i)$$

(omitting the kinematic term)

$$\mathbf{q} = \mathbf{k}_0 - \mathbf{k}_1$$

Replacing Electric field vector with q

Anisotropy effects

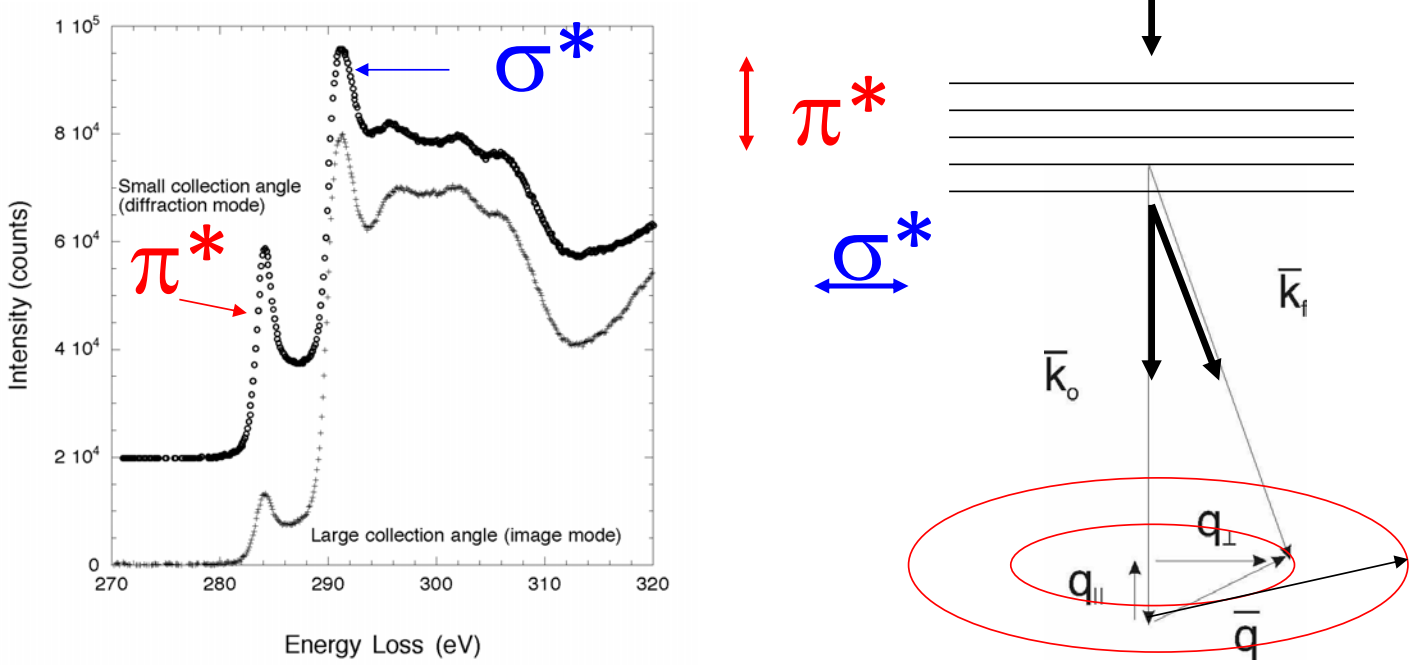

Initially observed for anisotropic materials (e.g. graphite). Also seen in BN, superconductors.

The effect is caused by the angular dependence of the electronic structure and the choice of experimental conditions. The scattering vector q points in different directions in the crystal and probes different portions of the bonds.

The same effect is observed in XAS. With photons the transitions are probed along the electric field vector (perpendicular to the beam direction). In EELS there is a larger flexibility as the scattering vector can be also changed (and momentum transfer is also large).
G.A. Botton, J. Electron Spectroscopy and Related Phenomena, 2005

Angular Distribution: Electron Scattering

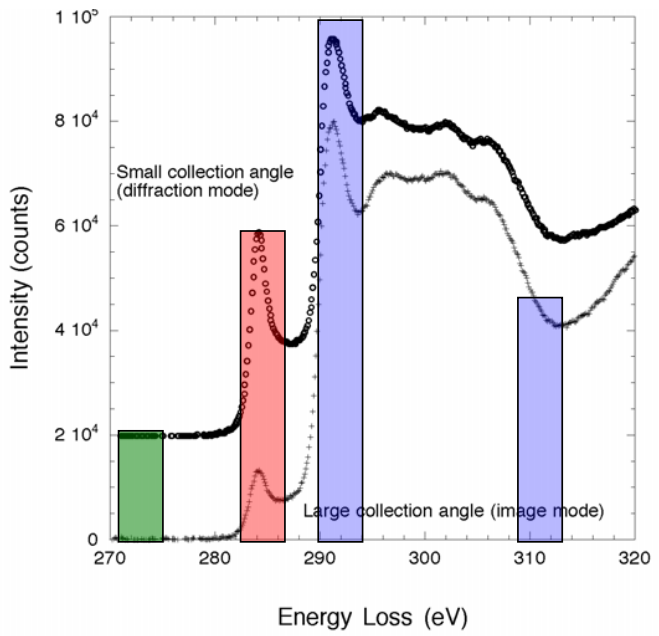

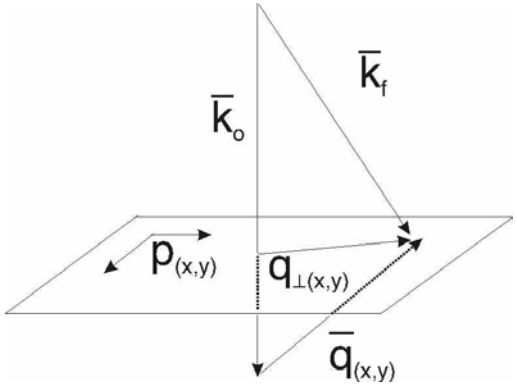

π^* σ^*

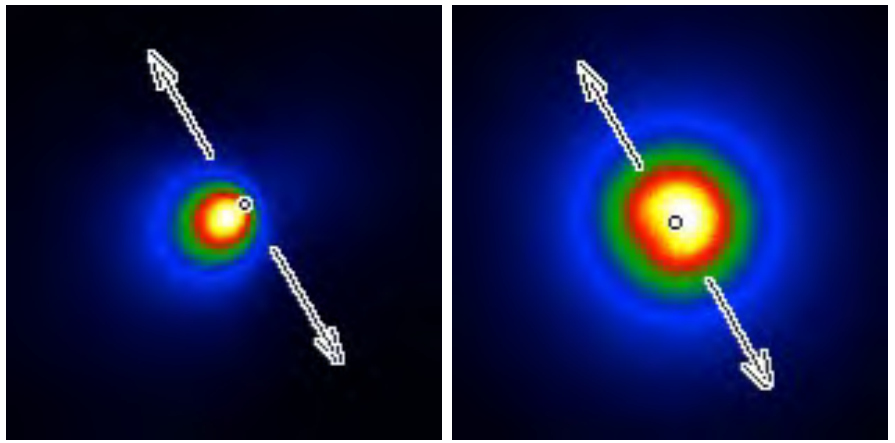

Botton, J. El. Spec. Rel. Phen. 2005

Opportunities (Synchrotron and EELS)

- 1) Intermediate states in reactions: full chemistry and not the ionic formal bond picture: not the bulk sample, the real one with full electron transfers with environment
- 2) excited states, will full angular dependence, phonon coupling effects, electron correlations

$SrTiO_3$ surfaces

Near Edge Structures from Surfaces?

diamond

Diamond-II | Advancing Science

Formation of a c(4x2) Surface Reconstruction

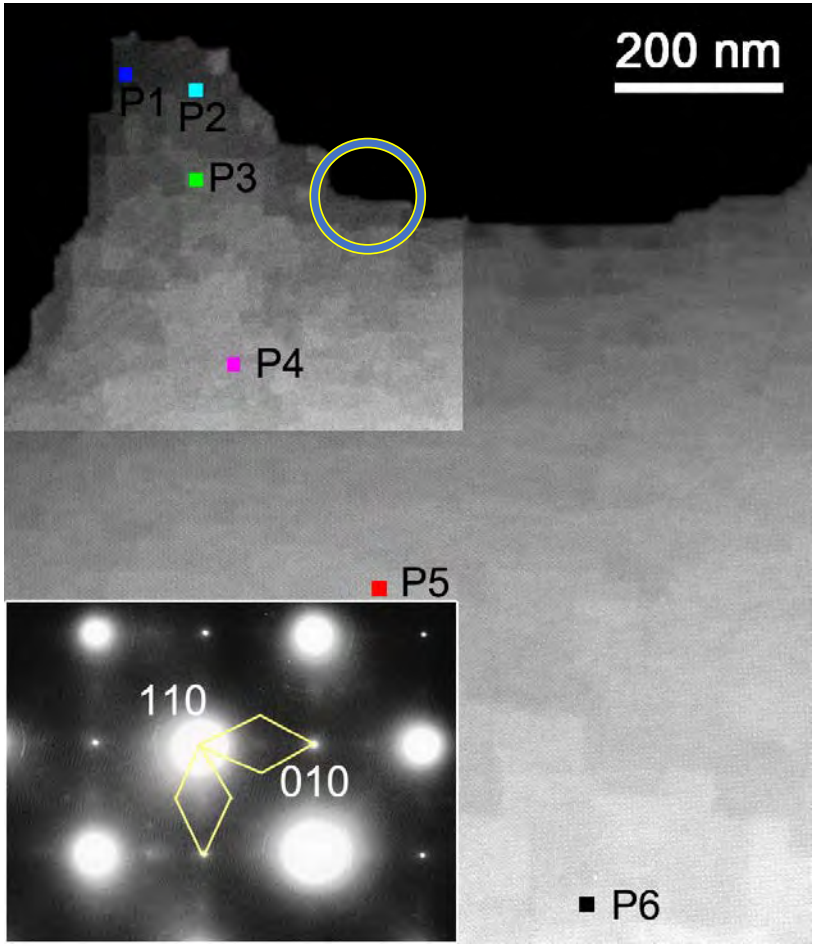

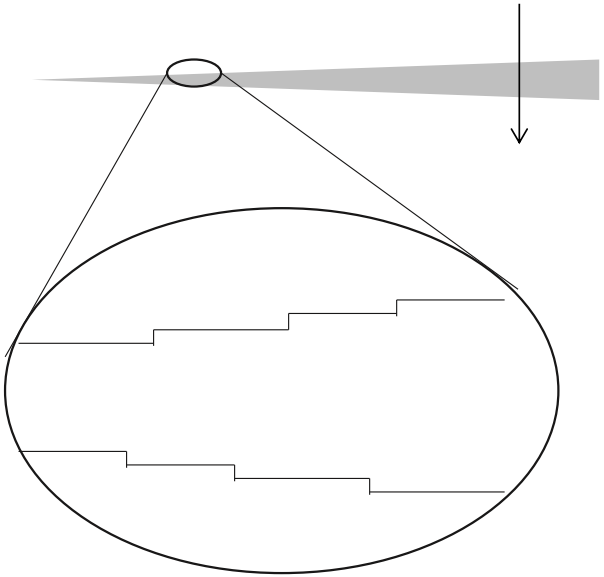

900˚ Annealed

Specimen preparation approach from Erdman 2002

Profile Images with Atomic Resolution

{100} sets of planes

- Topmost layer: a layer with a significant rearrangement
- Subsurface layer: a Ti-O layer
- Spacing: 0.24 nm

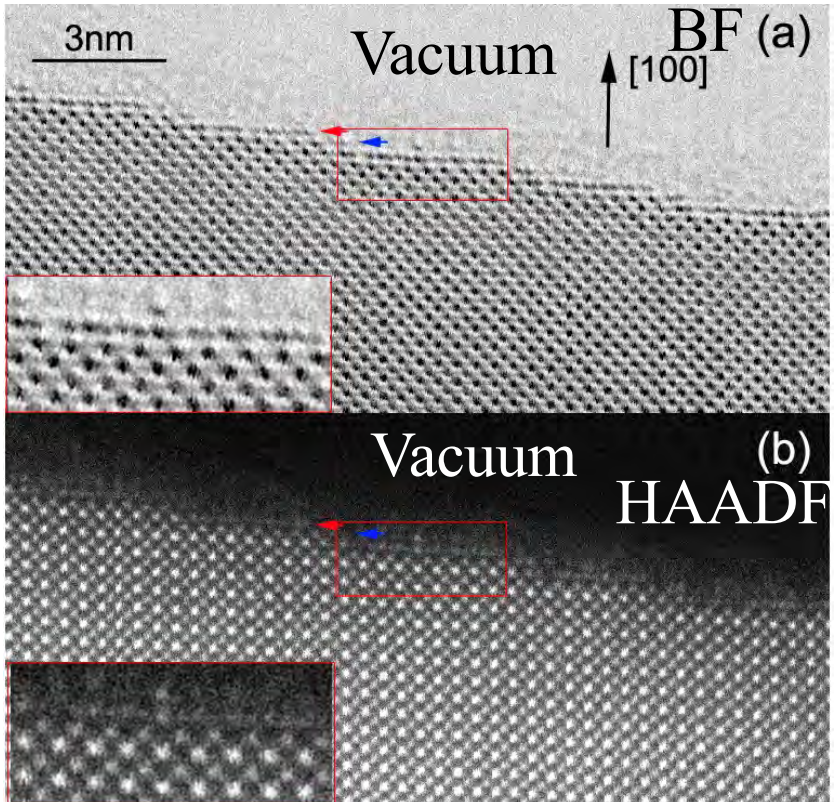

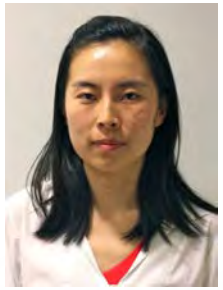

Guo-Zhen Zhu

diamond

Atomic model (type B) from Erdman 2003
Multislice simulation codes by Kirkland 2010

Diamond-II | Advancing Science

Crystal Field Effects on Ti L-edge EELS

Crystal Field Multiplet Simulation

- Topmost layer: TiO_5 units with charge transfer effect (from DFT)
- Subsurface layer: distorted TiO_6 units
- Subsequent layers: bulk signatures

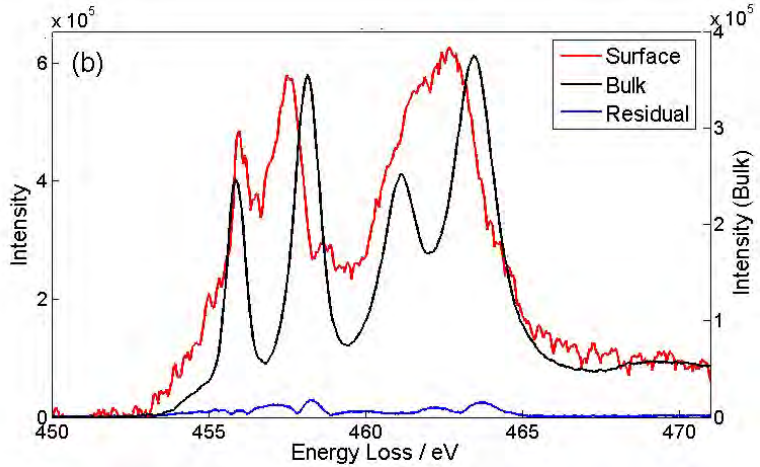

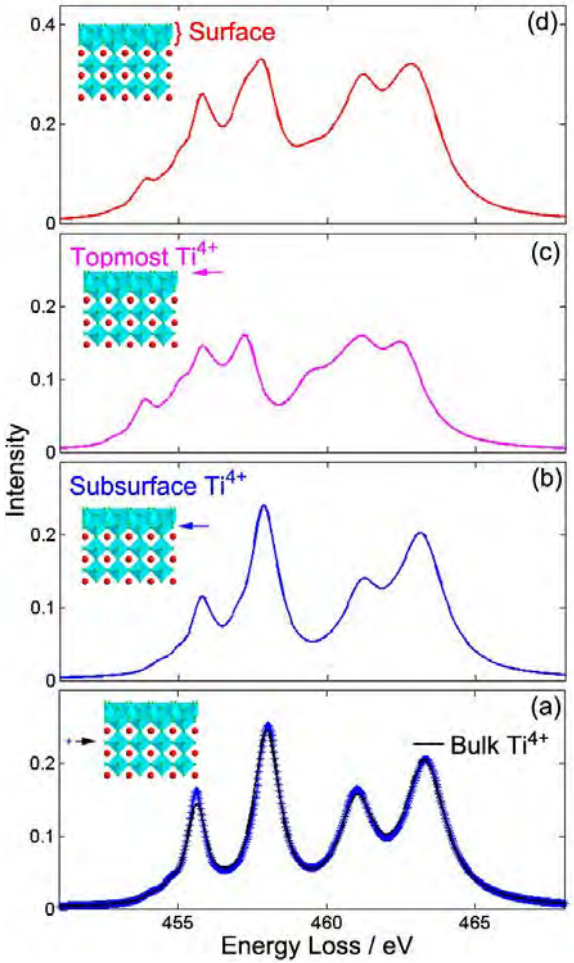

Multiplet codes by Uldry 2012
Atomic model from Erdman 2003

diamond

G-Z Zhu, G. Radtke, G.A. Botton, Nature, **490**, 384–387, 2012 , doi:10.1038/nature11563 , detailed methodology M&M 2014

Deductions from Model

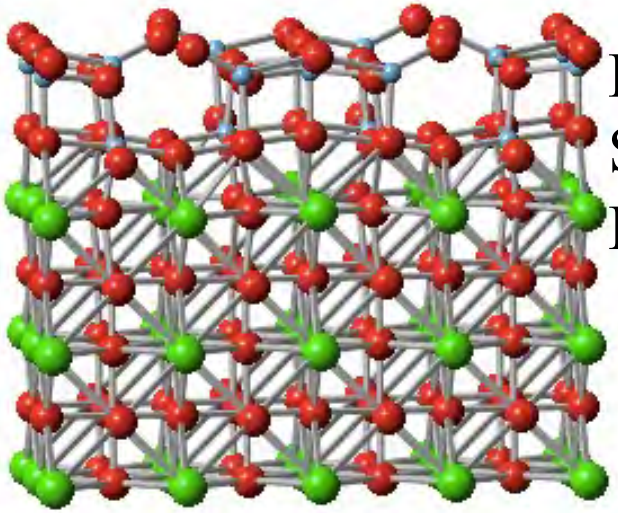

Detect distortions of octahedra,
Square pyramidal
Lower symmetry Ti and charge transfer

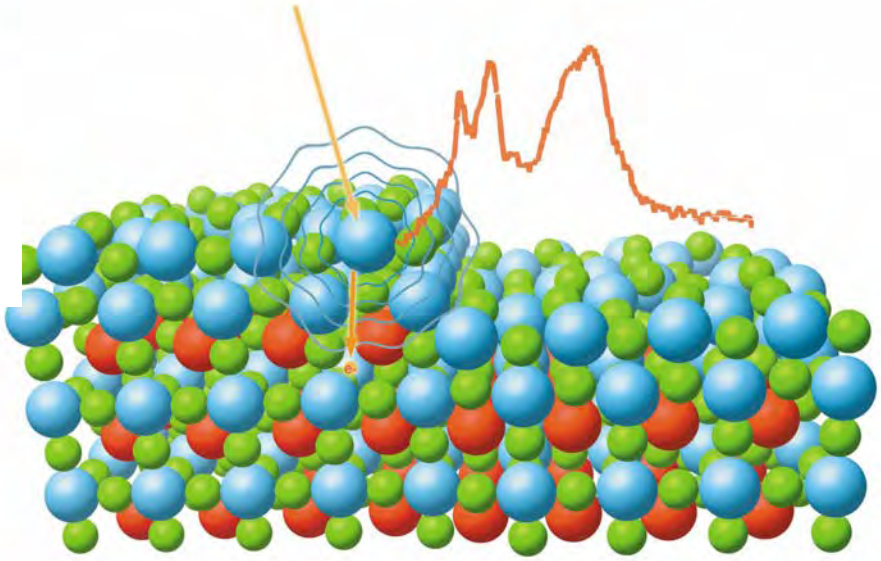

Ti^{4+} !!

G-Z Zhu, G. Radtke, G.A. Botton,
Nature, **490**, 384–387, (2012) doi:10.1038/nature11563

Chain-Ladder compounds

Localization of holes

Matthieu Bugnet
(now CNRS, Lyon)

Diamond-II | Advancing Science

Hole distribution in chain-ladder $Sr_3Ca_{11}Cu_{24}O_{41}$ superconductor

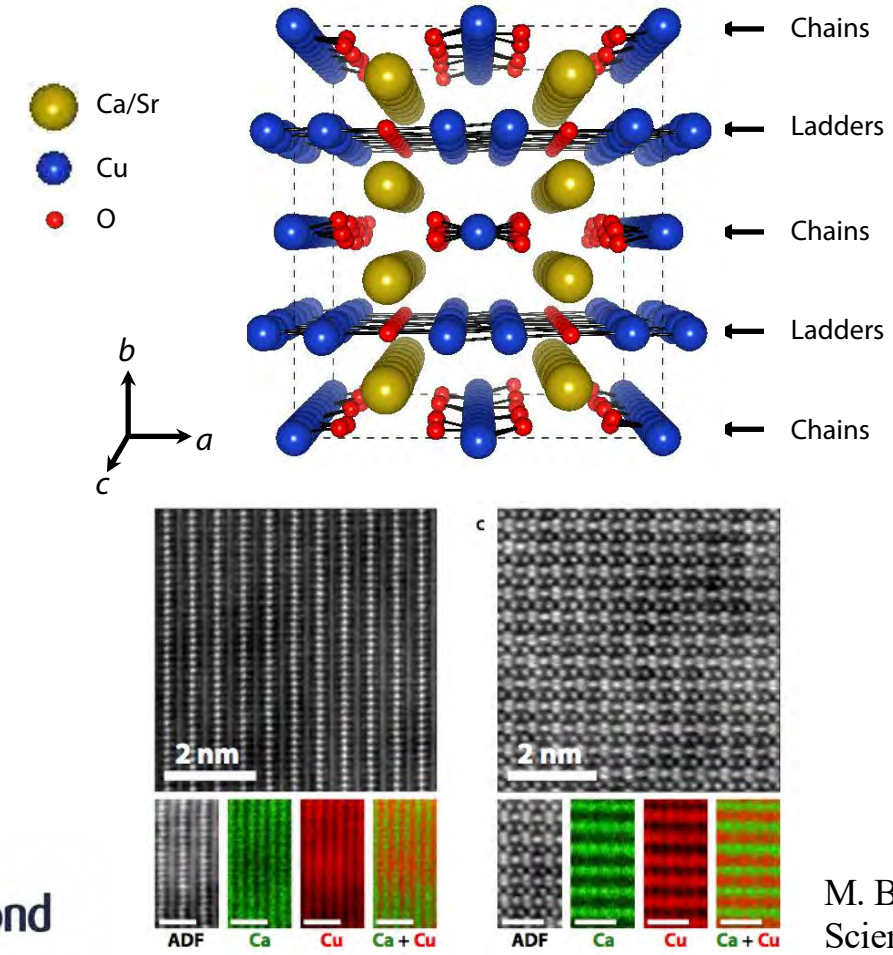

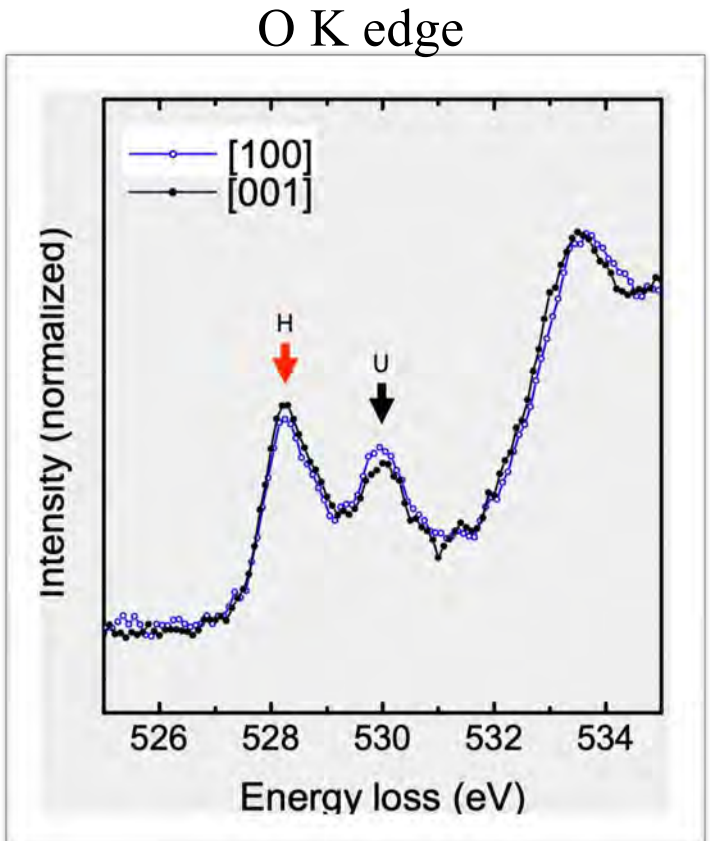

M. Bugnet G. Radtke, S. Loeffler, et al,
Science Advances, 25 March 2016 DOI: 10.1126/sciadv.1501652

Bulk

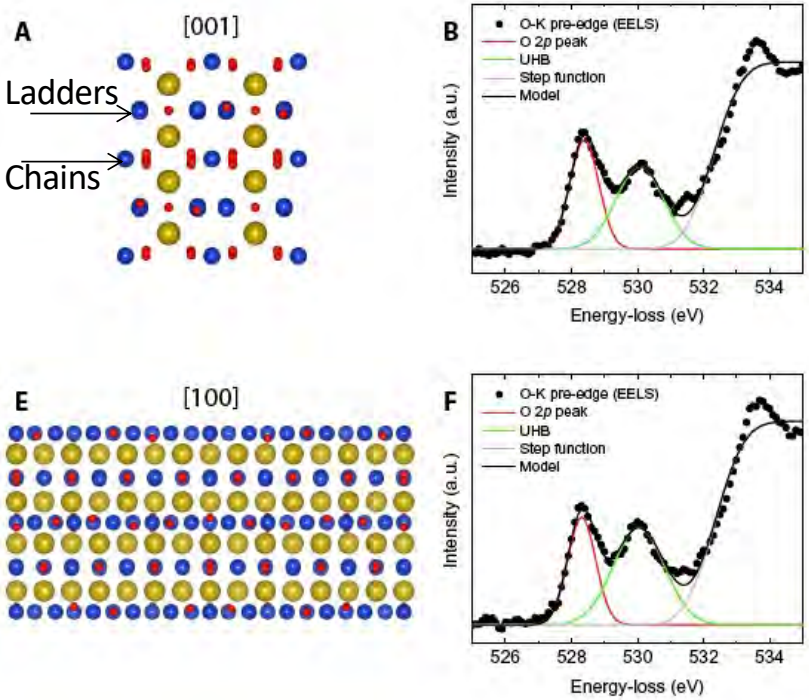
A
[001]
Ladders
Chains
B
O-K pre-edge (EELS)
O 2p peak
UHB
Step function
Model
Intensity (a.u.)
526
528
530
532
534
Energy-loss (eV)
E
[100]
F
O-K pre-edge (EELS)
O 2p peak
UHB
Step function
Model
Intensity (a.u.)
526
528
530
532
534
Energy-loss (eV)

Hole distribution in chain-ladder

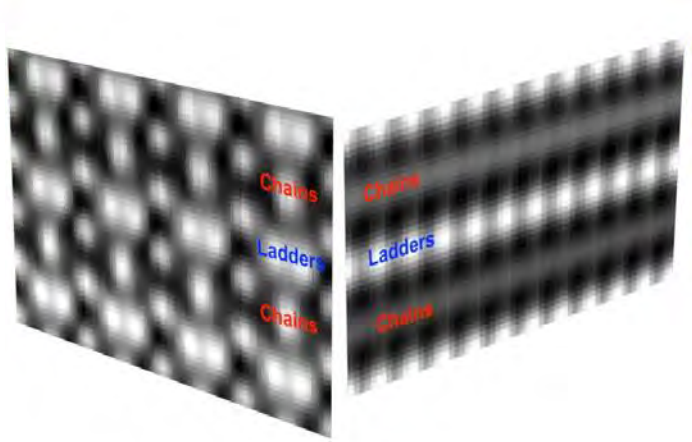

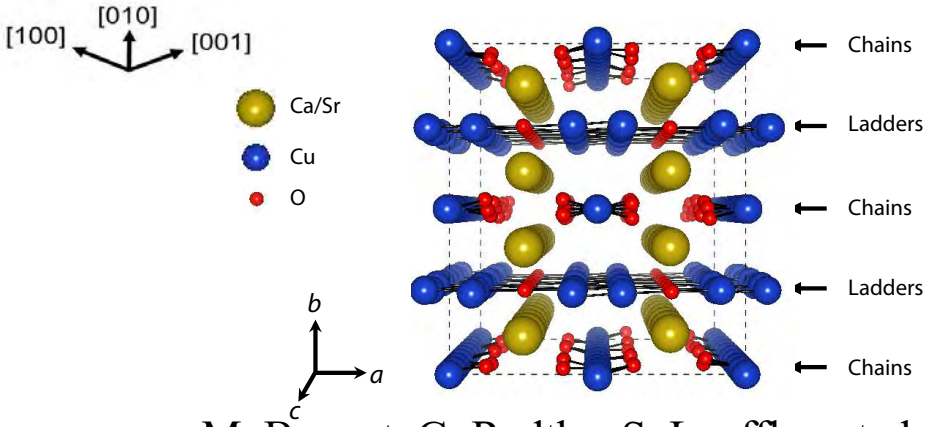

M. Bugnet G. Radtke, S. Loeffler, et al, Science Advances, 24 March 2016

diamond

Hole distribution in chain-ladder $Sr_3Ca_{11}Cu_{24}O_{41}$ superconductor

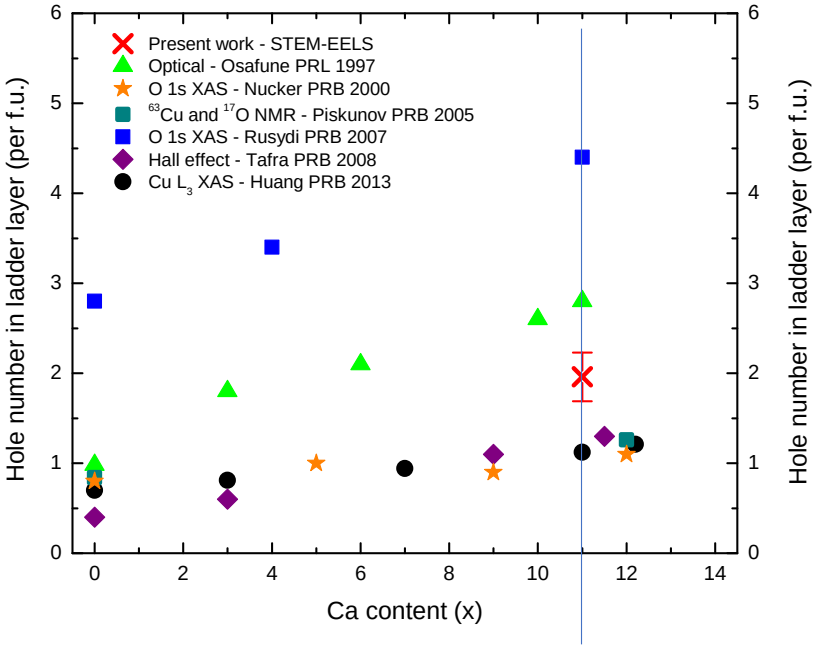

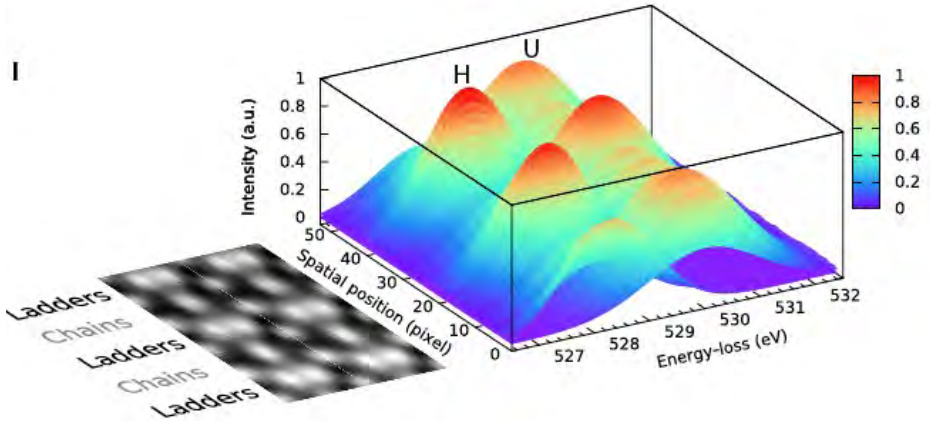

	Ladders	Chains
[100]	1.99 ± 0.28	4.01 ± 0.28
[001]	1.92 ± 0.26	4.08 ± 0.26

Applications

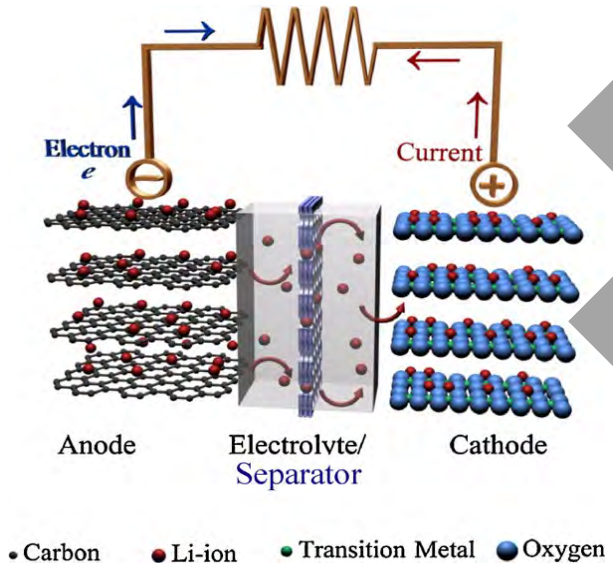

1. EELS study on charge compensation during cycling

2. Structural evolution of the cathode materials

NMC ($LiNi_{1/3}Mn_{1/3}Co_{1/3})O_2$

HE-NMC ($Li_{1.2}Ni_{0.13}Mn_{0.54}Co_{0.13}O_2$)

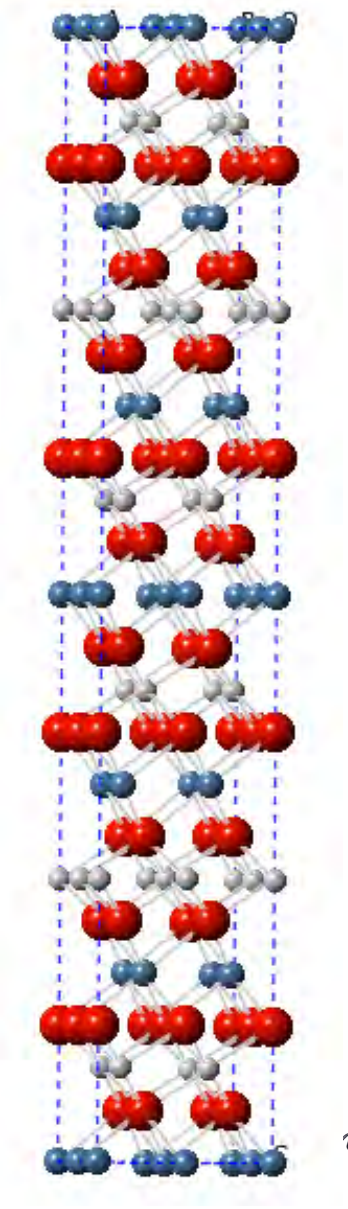

Diam ng Science

Charge Compensation?

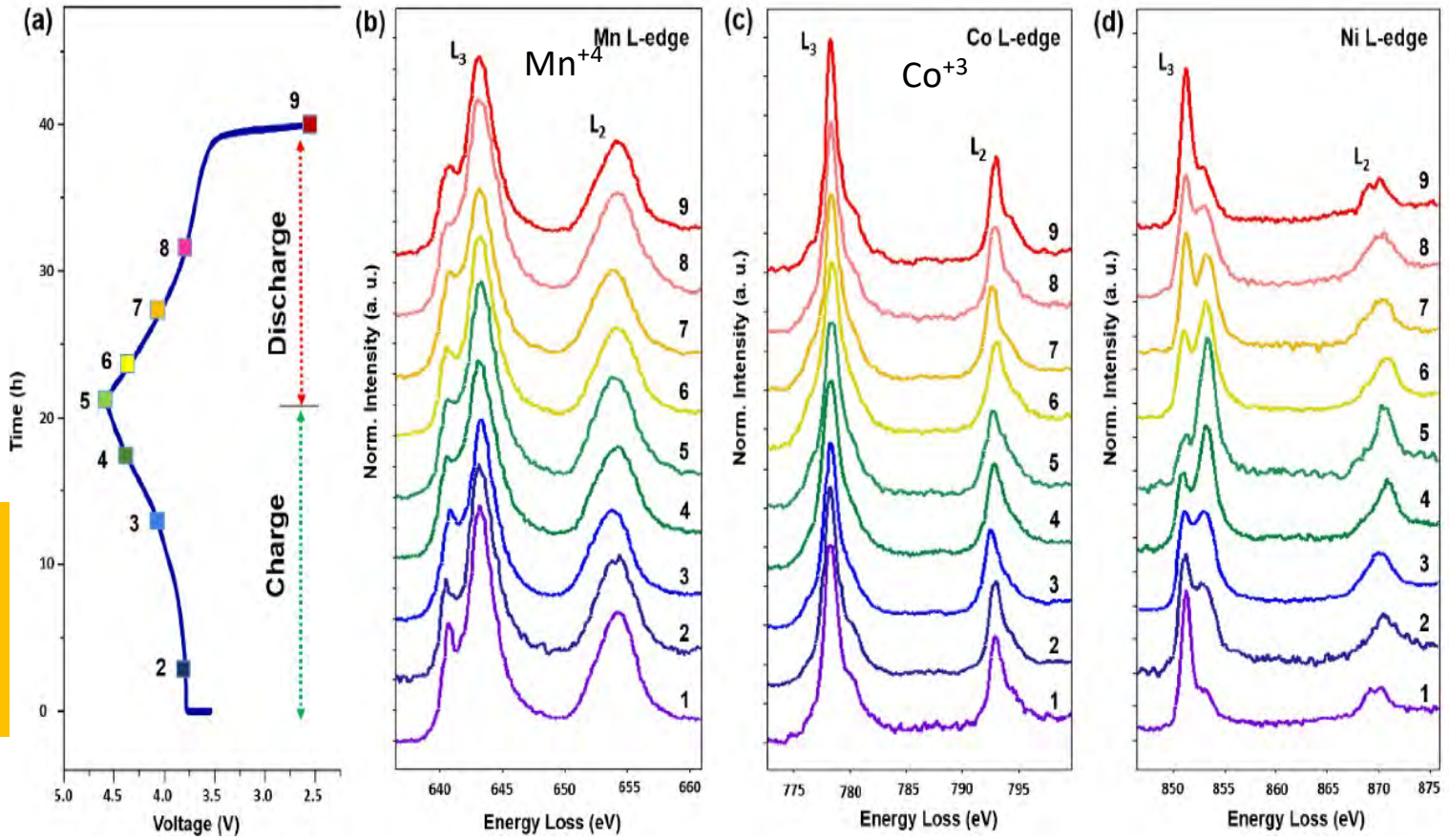

Hanshuo Liu, *et al.* Phys Chem. Chem. Phys.2016, DOI: 10.1039/c6cp05262b

During Li+ deintercalation:
Mn & Co — not being oxidized, Ni — $Ni^{2+} \rightarrow Ni^{4+}$

During Li+ intercalation:
Ni — $Ni^{4+} \rightarrow Ni^{2+}$

Ni 2+ → 3+? Or 4+?
Co, Mn unchanged.

Valence map of Mn and Co of 4.1V charged NMC

Vacuum transfer of sample in TEM

Valence map of Mn and Co of 4.1V charged NMC

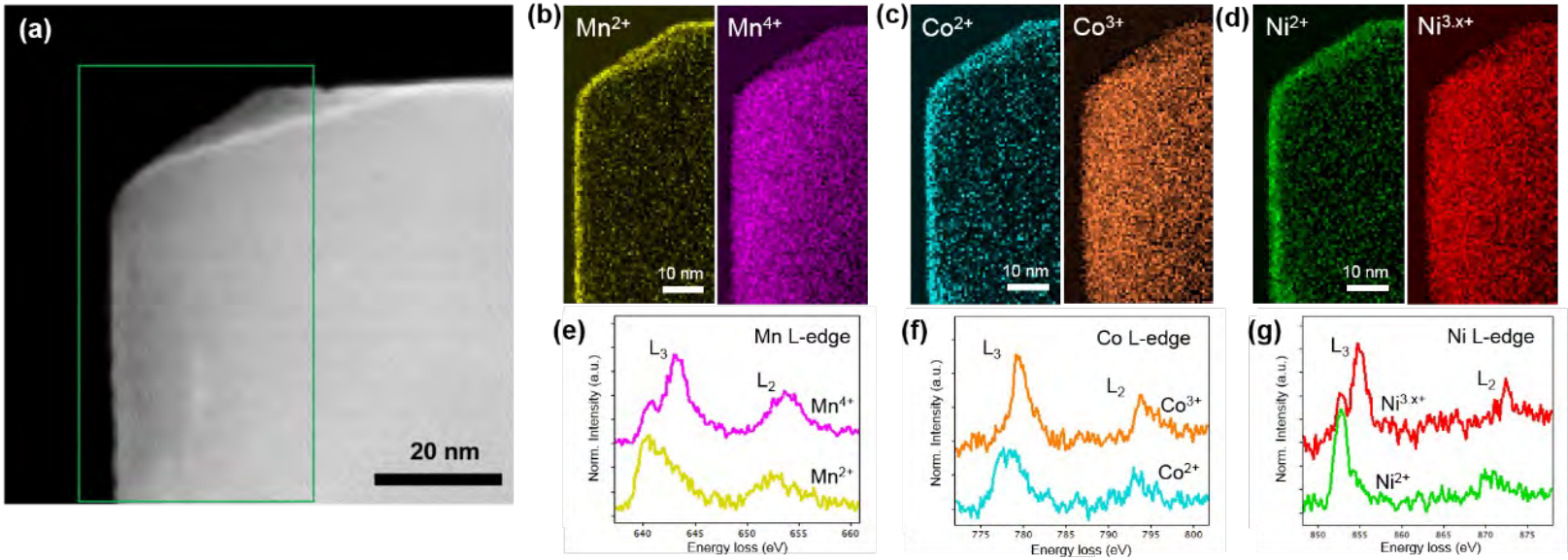

Liu *et al.*, Phys.Chem.Chem.Phys., 2016, 18, 29064

Surface reduction layer ~1.5 nm thick.
Electrochemical reduction only after electrolyte interaction, charging

HAADF-STEM image of a 4.1V charged NMC particle

diamond

Diamond-II | Advancing Science

Surface Reduction:
Charge Transfer with Electrolyte

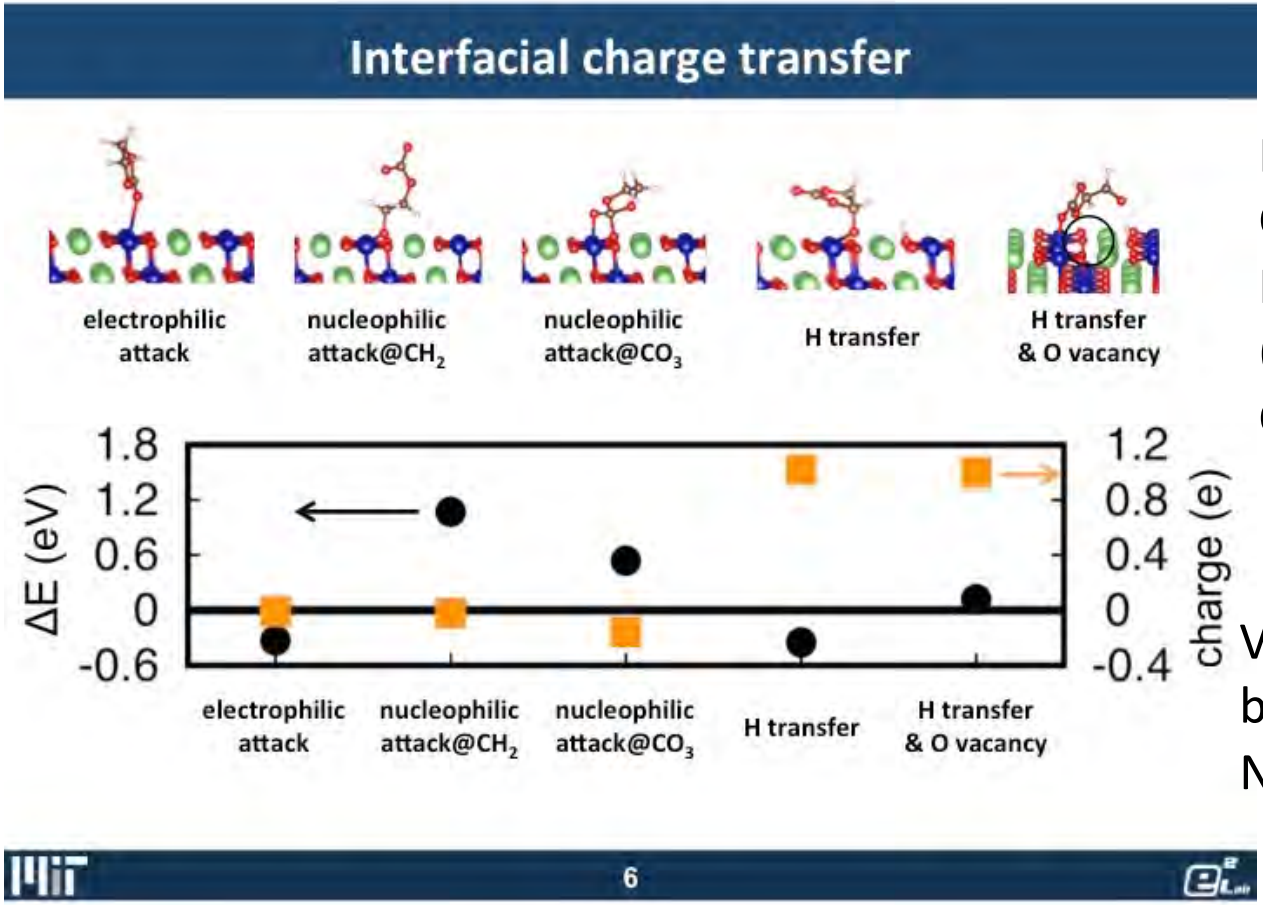

LMO Compounds In EC (Ethylene Carbonate)

Values might be different in NMC

From work of L. Giordano and Y. Shao-Horn, MIT

EELS spectra: 4.1V Charged State

- Ni has been oxidized to higher valence up to 4+.
- Ni is in lower valence at the surface (<3+) compared with the bulk (~4+) when probing perpendicular with Li^+ plane direction.

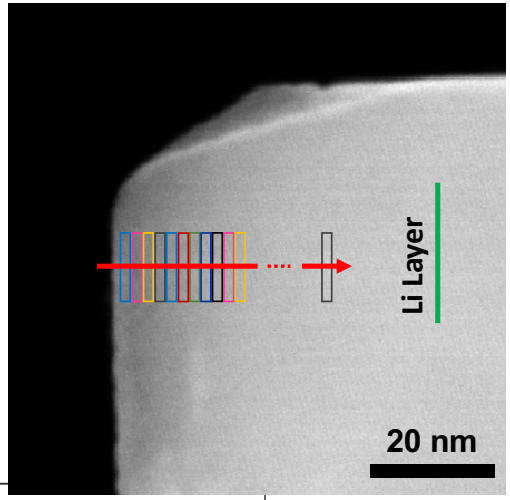

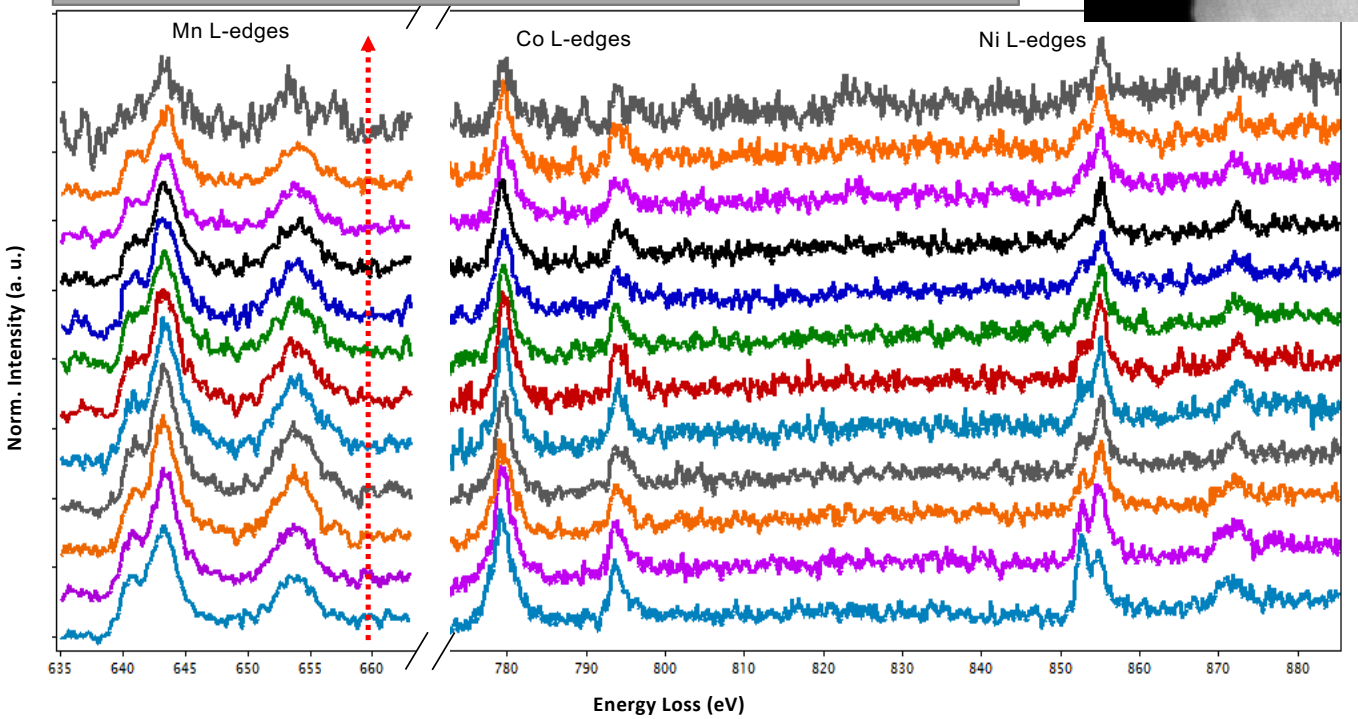

Cycling-induced Structural Evolution

STEM image of NMC after 20 cycles and the corresponding nanobeam convergent beam electron diffraction (CBED) pattern

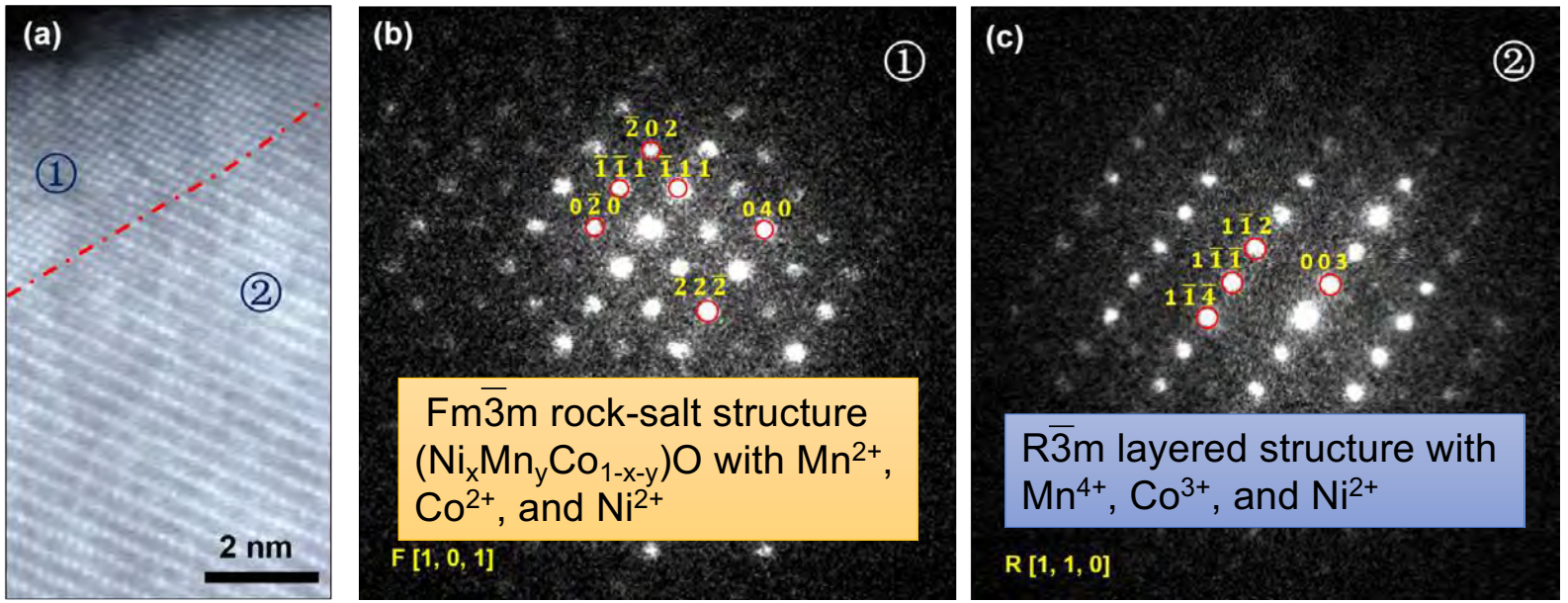

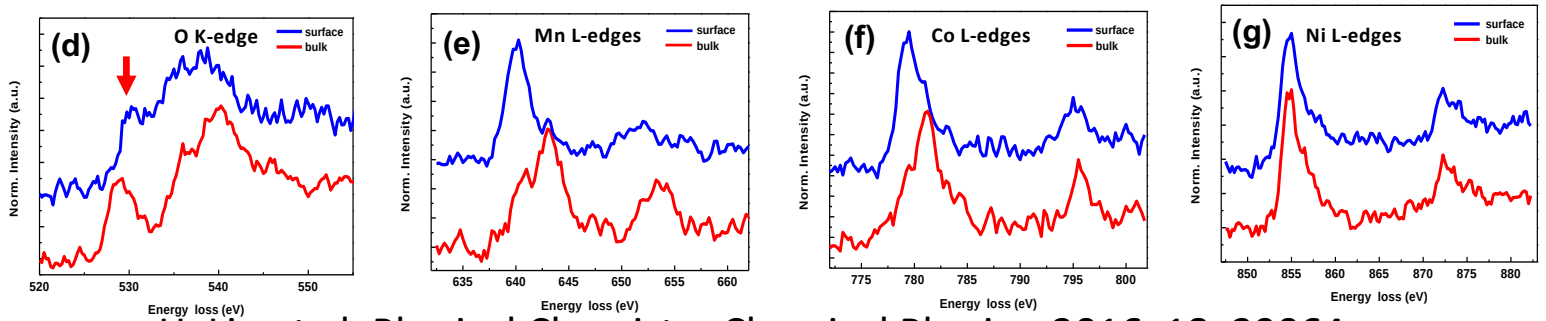

H. Liu et al, Physical Chemistry Chemical Physics, 2016, 18, 29064

Summary: Opportunities

- 1) Intermediate states in reactions: full chemistry and not the ionic formal bond picture: not the bulk sample, the real one with full electron transfers with environment.
- 2) Excited states, will full angular dependence, phonon coupling effects, electron correlations, beyond DFT to extract full details from spectra.
- 3) Local electronic structure (interfaces, become more dominant): supercell calculations, not bulk.

Challenges

- 1) Not just bulk spectroscopy but the interaction in an active environment, intermediate reactions (beyond DFT)
- 2) Massive data deluge even for spectroscopy (time, space)
- 3) Size of supercells for calculations
- 4) finally, you will see the damage, just as with electrons

Acknowledgements

- Diamond:
  - David Burn, Giannantonio Cibin, Sarnjeet Dhesi, Sofia Diaz-Moreno, Joshua Elliott, Diego Gianolio,, Ke-Jin Zhou,
- McMaster
  - : former students and collaborators over 20+ years.